Death induced by survival gene elimination (DISE) contributes to neurotoxicity in Alzheimer's disease

Bidur Paudel[1,10], Si-Yeon Jeong[1,10,11], Carolina Pena Martinez[2], Alexis Rickman[2], Ashley Haluck-Kangas[1], Elizabeth T. Bartom[3,4], Kristina Fredriksen[5], Amira Affaneh[5], John A. Kessler[5], Joseph R. Mazzulli[5], Andrea E. Murmann[1], Emily Rogalski[6,7], Changiz Geula[6,7], Adriana Ferreira[8], Bradlee L. Heckmann[2], Douglas R. Green[9], Katherine R. Sadleir[5], Robert Vassar[5, 6], and Marcus E. Peter[1,3,*]

*Correspondence: Marcus Peter, E-mail: m-peter@northwestern.edu, phone: 312-503-1291; FAX: 312-503-0189.
[1]Department of Medicine/Division Hematology/Oncology, [3]Department of Biochemistry and Molecular Genetics, Feinberg School of Medicine, Northwestern University, Chicago, IL

Full list of author information is available at the end of the article

[10]Shared first authorship

Abstract

Background: Alzheimer's disease (AD) is characterized by progressive neurodegeneration, but the specific events that cause cell death remain poorly understood. Death Induced by Survival gene Elimination (DISE) is a recently discovered powerful cell death mechanism mediated by short (s) RNAs including micro (mi) RNAs acting through the RNA induced silencing complex (RISC). G-rich 6mer seed sequences in the sRNAs (position 2-7) target hundreds of C-rich seed matches in genes essential for cell survival resulting in the simultaneous activation of multiple cell death pathways. The RISC of most cells is occupied by miRNAs with nontoxic 6mer seeds, which may protect them from DISE by blocking loading of toxic sRNAs. However, during aging when miRNA expression decreases, toxic sRNAs may enter the RISC more readily leaving cells primed for DISE. Whether DISE contributes to neuronal loss in a neurodegenerative disease such as AD has not been evaluated.
Methods: Using Ago precipitation and RNAseq (Ago-RP-Seq) combined with SPOROS, a recently developed bioinformatics pipeline to analyze small RNAseq data with respect to 6mer seed toxicity, we analyzed RISC bound sRNAs (R-sRNAs) in *in vitro* models and in the brains of multiple *in vivo* AD mouse models, aged mice, and AD patients.
Results: We find that in *in vitro* cell line studies, in mouse models that show neurodegeneration, and in the aging brain R-sRNAs shift to more toxic seeds. In contrast, in cells that survived in post-mortem brains of AD patients and the brains of "SuperAgers", individuals over age 80 who have superior memory performance, R-sRNAs shift to more nontoxic seeds, supporting a protective function of miRNAs.
Conclusion: Our data provide first evidence of a contribution of DISE to the neurotoxicity seen in AD suggesting that increasing the levels of protective miRNAs in the brain or blocking the activity of toxic R-sRNAs could lead to a novel way of treating the disease.

Keywords: DISE, Tau, neurotoxicity, RNAi

Background

Alzheimer's disease (AD) accounts for 50% - 75% of all dementia cases, and is primarily a condition of later life, roughly doubling in prevalence every 5 years after age 65 [1]. The worldwide incidence of AD is increasing with estimates that 115 million people will have AD by 2050. With an aging population this will create an unsustainable health care challenge if an effective treatment cannot be found. AD is characterized by a progressive occurrence of amyloid-beta (Aβ) plaques, neurofibrillary tangles (NFT), gliosis, and neuronal loss [2]. Many mechanisms and concepts have been proposed to explain the pathology of AD. Plaques, composed of Aβ, and accumulation of hyper-phosphorylated tau protein (p-Tau) into filaments and eventually NFT are at the base of the AD pathology [3]. Diseases characterized by the formation of NFT, tauopathies, are a large and diverse group of neurodegenerative disorders, that includes AD [4].

Neuronal loss characterizes the end stage AD pathology and hence cell death has been implicated in AD. It is often associated with either inflammation [5] and/or oxidative stress and superoxide production that can lead to neurodegeneration [6] through activation of multiple cell death pathways including apoptosis, necroptosis, autophagy, and parthanatos [7]. In fact, in all models of neuronal dysfunction, whether it is hyperactivity or neuronal silence resulting in cognitive impairment, neuronal dysfunction may also lead to cell death [8]. The multiple cell death pathways are believed to be evoked by excess amount of Aβ, caused by an increase in intracellular Ca^{2+} levels, oxidative stress, and receptor-mediated activation of cell-death cascades [9]. Toxicity by amyloid precursor protein degradation fragments such as Aβ42 is also well established [10, 11] and a strong genetic association exists between early-onset familial forms of AD (FAD) and Aβ42 (see [12-14]).

RNA interference (RNAi) is a form of post-transcriptional regulation exerted by 19-25 nt long double stranded (ds) RNAs that negatively regulate gene expression at the mRNA level. The active guide strand incorporates into the RNA induced silencing complex (RISC) [15] and the inactive passenger strand is degraded [16]. Once in the RISC the outcome of gene silencing depends on the degree of complementarity between the RISC-bound guide and the target mRNA [17]. The physiological way to induce RNAi is mostly mediated via miRNAs. They silence with the help of only a very short region of complete complementarity, the so called seed at positions 2-7/8 of the miRNA guide strand [18, 19]. Matching complementary regions (seed matches) predominantly located in the 3' untranslated region (3'UTR) of mRNAs are targeted [20, 21] resulting in cleavage-independent translational silencing [22]. This seed based targeting can be initiated with as little as six nucleotide long base-pairing between a guide RNA's 6mer seed and the targeted mRNA [18, 19]. miRNAs are transcribed in the

nucleus as primary miRNA precursors (pri-miRNA) [23] which are first processed by the Drosha/DGCR8 microprocessor complex into pre-miRNAs [24], and then exported from the nucleus to the cytoplasm by exportin 5 [25]. Once in the cytoplasm, Dicer/TRBP processes them further [26, 27] and these mature dsRNA duplexes are then loaded onto Argonaute (Ago) proteins to form the RISC [15]. Consequently, the deletion of either Drosha or Dicer results in the loss of almost all miRNAs [28, 29].

We previously discovered that a large number of si- and shRNAs were toxic to cancer cells independent of hitting their intended target [30]. Cells died of simultaneous activation of multiple cell death pathways [30]. Subsequently, we found that the RISC component Ago2 was required for cells to die, and that the toxic si/shRNAs acted like miRNAs by targeting the 3'UTRs of a network of essential survival genes [31]. We therefore called this phenomenon DISE (for death induced by survival gene elimination). This toxicity is dependent on targeting by only a 6mer seed [31]. Guide strand specific screens of siRNA duplexes carrying every possible 6mer seed (4,096 in total) revealed that the most toxic 6mer seeds are universally high in G nucleotides at the 5' end of the seed independent of tissue origin ([29, 32] and 6merdb.org). 6mer seed toxicity kills cells by targeting C-rich seed matches located in the 3'UTR of an assortment of essential survival genes. Consequently, the most abundant miRNAs are devoid of G-rich seeds [29] likely to prevent the downregulation of essential survival genes which would result in the death of the cell. This concept is also supported by the previous observation that genes essential for cell survival have been evolutionarily selected to be devoid of seed matches for abundant miRNAs [33]. Thus, we discovered a “kill code” embedded in the genome with the potential to induce rapid and inescapable cell death. We reported that certain tumor suppressive miRNAs (e.g. miR-34a/b/c-5p or miR-15/16-5p) use this mechanism to kill cancer cells and that the kill code is at least 800 million years old [29, 34]. More recently, we developed SPOROS, a bioinformatics tool to aid in the study of the role of this “kill code” in cell death more broadly. SPOROS is a standardized, semi-automated pipeline to analyze seed toxicity of sRNAs in a gene agnostic fashion [35].

Based on these findings, we recently postulated that normal cells are protected from 6mer seed toxicity by multiple mechanisms [36]. One of them involves large quantities of miRNAs carrying nontoxic seeds that are expressed at high levels in normal but not cancer tissues [37-40]. Consistently, we found that global downregulation of most abundant miRNAs, which carry mostly nontoxic seeds, caused by deleting either Dicer or Drosha sensitizes cells to effects of toxic sRNAs [29, 31, 38, 41]. These results posed the question of what happens if a normal tissue loses its miRNA protection.

We now demonstrate that DISE may contribute to neuronal cell death in AD. Our data demonstrate that exposure of differentiated SH-SY5Y (SH) cells to Aβ42 oligomers results in an increase of RISC bound sRNAs (R-sRNAs) with more toxic seeds and that cells with reduced ability to produce most miRNAs (e.g. lacking Drosha expression) are hypersensitive to sRNAs with toxic seeds. In addition, inhibiting RISC function blocks the toxicity of Aβ42. Supporting the contribution of DISE to neurotoxicity seen in AD we show that in the two of the three mouse models of AD that exhibit neuronal cell death, the median seed viability of R-sRNA in brains is reduced. In contrast, in postmortem brains of AD patients we found an increase in seed viability of R-sRNAs potentially due to the fact that the analyzed cells of these brains were the ones that survived years of ongoing AD and hence were more resistant to neurotoxicity. This interpretation was supported by a kinetic analysis of R-sRNAs in Aβ42-treated differentiated SH cells and in an analysis of induced pluripotent stem cell (iPSC) derived neurons from normal control and AD patients. Finally, we provide evidence for the role of miRNAs in protecting aging brains from DISE as the aging mouse brain loses expression of protective miRNAs. In addition, R-sRNAs from brains of a group of old individuals (>80 years) with memory capacity of 50-60 year-olds (SuperAgers) have a higher seed viability than R-sRNAs in the brains of age-matched control individuals.

In summary, we provide first evidence of a contribution of DISE to the neurotoxicity seen in AD suggesting that increasing the levels of protective miRNAs in the brain could lead to a novel way of treating the disease.

Methods

Reagents and antibodies

The following reagents and antibodies were used (sources given in brackets): Dibutyl cyclic AMP (dbcAMP) (Sigma Aldrich #D0260), *all-trans* retinoic acid (RA) (Sigma Aldrich #R2625), Brain-derived neurotrophic factor (BDNF) (GeminiBio #300-104P), Amyloid β-Protein (Aβ42) trifluoroacetate salt (Bachem #H-8146.5000), Amyloid β-Protein (Aβ40) trifluoroacetate salt (Bachem #H-1194.5000), Aurintricarboxylic Acid (ATA) (Sigma Aldrich #189400), Opti-MeM (Thermo Fisher Scientific #31985088), Lipofectamine RNAimax (Thermofisher Scientific #56532), Lipofectamine 3000 (Thermofisher Scientific #100022052), 1,1,1,3,3,3-Hexafluoro-2-Propanol (HFIP)(Sigma Aldrich #105228), Argonaute-2 Rabbit pAb (Abcam #ab32381), Tyrosine Hydroxylase

Rabbit pAb (TH)(Cell Signaling #2792), GAP43 (D9C8) Rabbit mAb (Cell Signaling #8945), Tau-1 Mouse mAb (Millipore Sigma #MAB3420), Drosha (D28B1) Rabbit mAb (Cell Signaling #3364), Goat Anti-Rabbit 2°Ab (Southern Biotech #4030-05), Goat Anti-Mouse 2°Ab (Southern Biotech #1070-05), HRP-conjugated β-Actin (C4) Mouse mAb (Santa Cruz Biotechnology #Sc-47778), Phospho-Histone H2A.X (Ser139) (20E3) Rabbit mAb (Cell Signaling #9718). Neuronal class III β tubulin (TUJ1) (mAb Covance #MMS-435P, 1:2000), LMX1A (pAb, Merck-Millipore #AB10533, 1:1000), Tyrosine Hydroxylase (pAb, Merck-Millipore #657012, 1:1000), HNF-3 beta (FOXA2) (mAb, Santa Cruz # sc-101060, 1:100).

Aβ peptide preparation

Solubilization, stock preparation and oligomerization of Aβ42 was performed as previously described [42, 43] with some additional modifications. Briefly, lyophilized Aβ42 was allowed to equilibrate at room temperature for 30 min and resuspended in ice cold HFIP under fume hood to obtain 1 mM solution. To disintegrate previously formed random oligomers and achieve complete monomerization, solution was vortexed vigorously for 1 min and kept at RT for 2 hrs. After monomerization, peptide solution is aliquoted in desired volumes into 1.5 ml microcentrifuge tubes, air dried overnight and then transferred to SpeedVac for another 2 hrs to remove traces of HFIP. Complete removal of HFIP and quality of monomer formation is validated by the formation of clear peptide film observed at the bottom of the tubes. Tubes containing peptide films were parafilmed and stored at -80°C for further use. For oligomerization, tube containing peptide film is dissolved in DMSO at 5 mM, vortexed for 30 sec and sonicated in the water bath for 10 min for complete suspension. Peptide is further diluted to 100 μM, vortexed, briefly centrifuged and kept at 4°C for 24 hrs for oligomer formation. Media to dilute peptide depended on the experimental condition and lacked FBS and phenol red components. After 24 hrs low molecular weight soluble peptide oligomers were retrieved by centrifugation at 14,000g for 10 min and applied at various concentrations in toxicity assays. To control for HFIP toxicity Aβ40 was prepared in the same manner as Aβ42.

Cell culture

Human neuroblastoma cell lines; SH-SY5Y (# CRL-2266^{TM}) (SH cells) were purchased from ATCC and NB7 were kindly provided by Dr. Jill Lahti (St. Jude Children's Research Hospital, Memphis, TN). SH cells were cultured in Dulbecco's Eagle's medium (DMEM) (Corning # 10-013-CM) and NB7 cells in RPMI 160 medium (Corning # 10-040-CM), both supplemented with 10% heat inactivated fetal bovine serum (FBS) (Sigma-Aldrich # 14009C, 1% L-glutamine (Corning # 25-005-CI) and 1% penicillin/streptomycin Corning # 30-002-CI). Cells were maintained at 37°C in saturated humidity atmosphere of 95% air and 5% CO_2.

Generation of Drosha k.o. NB7 cells

NB7 Drosha k.o. cells were generated using the Alt-R CRISPR-Cas9 System (IDT DNA Technologies) following the manufacturer's protocol with the following modifications. A paired set of sgRNAs, one targeting in exon 2 (IDT predesigned gRNA Hs.Cas9.DROSHA.1.AB GUACAAAGUCUGGUCGUGGA) and one targeting downstream of exon 32 (IDT custom design AUAACUUGAUGAACAGCCAC) were annealed with the Alt-R Crispr Cas9 tracrRNA 5' ATTP 550 (#1077024) and mixed 1:1. The sRNA mix (22 pmol) was incubated with 18 pmol Alt-R Cas9 Nuclease V3 (#1081058) diluted in Resuspension Buffer R (Invitrogen #MPK10025). The Invitrogen Neon Transfection System was used to transfect the Cas9-sgRNA complex into $2x10^5$ NB7 cells in 200 μL Resuspension Buffer R with Cas9 electroporation enhancer (1200 volts, 30 ms width, 1 pulse). The next day single PE^+ cells were sorted into 96-well plates and cultured for ~ 6 weeks. Knockout was confirmed by western blot.

Cell growth and viability assessment

Transfection of all cell lines (SH, NB7 and their Drosha k.o. clones) were performed in TPP 96 well plate (Millipore Sigma # 92696) in 250 μl final volume. Briefly, 50 μl Opt-MeM containing siRNA-lipofectamine RNAiMax (NB7) or siRNA-lipofectamine 3000 (SH) complex was forward transfected to 200 μl cells containing 3,000 NB7 cells/well or 6,000 SH cells/well. The optimized amount of lipofectamine RNAiMax or lipofectamine 3000 for both cell lines was 0.3 μl. siRNAs used to transfect these cells were siNT1, siGGCAGU, siGGGGGC or siCAG (sequences all with their guide strands modified by 2'-O-methylation of their positions 1 and 2 as previously reported [32, 38]). Following transfection, cell growth was monitored for at least 160 hrs in the IncuCyte Zoom live-cell imaging system (Essen Bioscience) with a 10X objective. The cell confluency curves were generated using IncuCyte Zoom software (version 2015A). To determine the presence of metabolically active cells after various treatments, ATP quantification was performed using Cell/Titer-Glo Luminescent Cell Viability Assay Kit (Promega # G7571). Following Aβ40/Aβ42 or ATA treatment in 96 black well plate, an equal volume of Cell

Titer-Glow reagent was added to the amount of cell culture media in the well. The contents were mixed in orbital shaker for 2 min to induce cell lysis and incubated for another 10 min to stabilize the luminescent signal. Subsequently, luminescence signal was recorded using microplate reader (BioTek Cytation 5).

Differentiation of SH cells

SH cells were differentiated into neuronal-like phenotypes by two methods as described previously, one by using dbcAMP [44] and other by the combination of retinoic acid (RA) and brain-derived neurotrophic factor (BDNF) [45, 46]. Briefly, SH cells maintained in DMEM media were seeded at a density of 10,000 cells/well in 96 black well plate. After 24 hrs, DMEM media was removed, and cells were differentiated with 1 mM dbcAMP in Nb-active no phenol red (BrainBits # NbActiv4-PR) media for 7 days. At day 5 of differentiation, undifferentiated cells were again seeded at same density in parallel. At day 7, when cells were differentiated they were treated with 20 μM (unless otherwise noted) Aβ40/Aβ42 for 48 hrs and ATP cell viability was measured as described before. To achieve neuron-like differentiation by RA/BDNF, cells were first pre-differentiated with 10 μM RA in complete DMEM media for 5 days and then treated with 50 ng/ml BDNF in the same media that lacked FBS and phenol red for additional 2 days. Seven days differentiated neuron-like cells were then used to assess toxicity of Aβ40/Aβ42 in all experiments involving differentiated SH cells.

Hydrogen peroxide treatment

NB7 and NB7 Drosha k.o. clones (A3-3, A3-11) were seeded in 96 black well plate (3,000 cells/well) in complete RPMI media. After 24 hrs cells were treated with 25 and 50 μM H_2O_2 for 3 hrs and allowed to recover for 21 hrs and ATP cell viability was measured as described above. To validate ATP data, another 96 black well plate with similar experimental design was run in an IncuCyte machine to monitor the effect of H_2O_2 on cell proliferation (data not shown).

Aurintricarboxylic acid treatment

Stock solution of ATA was prepared in 0.1 M NaOH. Prior to siRNAs transfection or treatment with Aβ42 cells were pretreated with indicated concentrations of ATA for 2 hrs and its presence was continued throughout the analyses.

Reactive oxygen species (ROS) measurement

Intracellular induction of ROS was monitored by 2',7' –dichlorofluorescin diacetate (DCFDA) cellular ROS assay kit (Abcam # ab113851) in accordance with manufacturer's recommendation. Briefly, 25,000 SH cells/well were seeded at least in triplicates in 96 black well plate and differentiated for 7 days. At day 7 cells were washed once with DMEM media (devoid of phenol red and FBS) and loaded with 10 μM DCFDA for 45 min at 37°C in the dark. Following incubation, DCFDA solution was removed, washed once, and treated with 20 μM Aβ40/Aβ42 for 4 h. To evaluate ROS induction, plate was read on a microplate reader at Ex/Em =485/535 nm in end point mode in the presence of Aβ40, Aβ42 or control media. ROS induction in NB7 cells were performed in a similar manner except DCFDA incubation was done in complete RMPI no phenol red media, and the cells were washed with 1X buffer provided in the kit.

RNA extraction, reverse transcription, and quantitative real time PCR

Monolayer of 1.0 x 10^6 cells grown in 6 well plate was lysed in 500 μl/well QIAzol Lysis Reagent (Qiagen #79306) and RNA extraction was performed with QIAzol miRNeasy Mini Kit (Qiagen #217004) according to manufacturer's instruction. All RNA samples were subjected to DNAse digestion using RNAse-free DNAse set (Qiagen #79256) and eluted in 35 μl ultra-pure H_2O. RNA quality control was performed with Nanodrop 2000c spectrophotometer. Subsequently, 100 ng RNA was reverse transcribed using High-Capacity cDNA Reverse Transcription Kit (Applied Biosystems # 4368813) in 15 μl. cDNA was further diluted in ultra-pure H_2O to 45 μl, and qPCR was performed with TaqMan Universal PCR Master Mix (Thermo Fisher scientific #4324020) using 5 μl cDNA in a 20 μl total volume. Assay was run on 7500 Real Time PCR System (Applied Biosystems). Small nucleolar RNA (Z30) (Thermo Fisher Scientific, #001092) that have been reported to show good abundance and relatively stable expression was used as an endogenous control. Primers used to quantify expression levels of miRNAs in Parental and Drosha k.o. clones were hsa-miR-21 (Thermo Fisher Scientific, #0003970), Let-7a (Thermo Fisher Scientific # 000377), hsa-miR-221 (Thermo Fisher Scientific #000524) and hsa-miR-182 (Thermo Fisher Scientific #002334). Relative expression of miRNAs run in triplicates were normalized to the levels of Z30 and expressed as $2^{-\Delta\Delta Ct}$.

Western blot analysis

Cell pellets containing ~1.0 x 10^6 cells were lysed in 250 µl RIPA buffer (150 mM NaCl, 10 mM Tris HCl pH 7.2, 1% SDS, 1% TritonX-100, 1% deoxycholate, 5 mM EDTA) supplemented with 1 mM PMSF and protease inhibitor cocktail (Roche #11836170001). To ensure complete lysis, cells were kept on ice for 30 min, vortexed occasionally and sonicated. Lysed cells were then boiled for 10 min at 95°C and centrifuged (14,000 rpm at 4°C) for 15 min. Protein quantification was performed with DC Protein Assay Reagent (BIO RAD) in an iMark Microplate Reader (BIO RAD) at 750 nm. 20 µg protein per lane was run on SDS-polyacrylamide gel electrophoresis (SDS-PAGE) (BIO-RAD #1610158) at 40 mA for ~1 h. Resolved proteins were then transferred to Nitrocellulose Blotting Membrane (Healthcare #10600016) at 250 mA for 2 hrs on ice. Transferred membranes were then blocked with 5% non-fat dry milk for 1 hr at room temperature in TBST (Tris-buffered saline, 0.1% Tween 20) and immunoblotted with various antibodies overnight (1:1000 in 3% BSA in TBST). Following primary antibody incubation, membranes were washed with TBST and probed with secondary Goat-anti-Rabbit or Mouse IgG HRP (1:5000 in 1% milk for 1 hr at RT). Finally, membranes were washed and developed with Super Signal West Dura Luminol/Enhancer (Thermo Scientific #1859025).

Western blot analysis of iPSC derived midbrain dopamine neurons: Cultures were harvested at different time points as indicated in the figures and lysed in 1% Triton X-100 buffer containing protease inhibitor cocktail (Roche diagnostics, # 11-836-170-001), 1 mM PMSF, 50 mM NaF, 2 mM sodium orthovanadate by homogenization and incubation on ice for 30 minutes. The protein concentration was determined by using micro-BCA kit (ThermoFisher, # 23235) and 40 µg of lysates were loaded onto 10% Tris/glycine PAGE gels followed by transfer onto PVDF membranes (EMD Millipore, # IPFL00010) at 30V for 1hr). Membranes were post-fixed in 0.4% paraformaldehyde, washed in milliQ water and then blocked in 1:1 TBS : odyssey blocking buffer (Licor # P/N 927-40003) for 1 hr at room temperature. The membrane was incubated with primary antibodies diluted in 1:1 ratio 0.2% TBS-tween and odyssey blocking buffer overnight at 4°C. The following day the membrane was washed with 0.2% TBS-Tween and incubated with secondary antibodies for 1 hr. Anti-rabbit IgG conjugated to IRDye800 and anti-mouse IgG conjugated to Alexa 680 were used for simultaneous detection of both channels on the same blot. The blot was washed as before and scanned on an odyssey imaging system. The western blots were analyzed using Image Studio software (Licor) to quantify band intensities.

Mouse and human brain tissue

5XFAD mice were bred in house by crossing 5XFAD transgenic males (line 6799) to B6/SJL F1 hybrid females and genotyped as described [47]. Mice were sacrificed by CO_2 inhalation. One hemibrain was snap-frozen in liquid nitrogen. Three transgenic and three non-transgenic females were used for analysis. 6 or 8 months old female 5XFAD Rubicon$^{+/-}$ or 5XFAD Rubicon$^{-/-}$ mice [48]; or 3 month old male control and Tau45-230 transgenic mice generated using the human cDNA coding sequence for tau45-230 under the control of the Thy 1.2 promoter on a C57BL/6J background [49].

Frozen brain tissue from the middle frontal gurus of 5 cognitively normal elderly participants, 7 clinically and pathologically confirmed AD patients [49, 50] and three cognitive SuperAgers were obtained from the Northwestern University Alzheimer's Disease Center Brain Bank. Brains of cognitively normal individuals were free of neurodegenerative pathology, except for age-appropriate accumulation of plaques and tangles [50]. SuperAgers participants were enrolled in the Northwestern University SuperAging Program, were 80 years or older, were required to perform on the Reys Auditory Verbal Learning test of episodic memory equal to or better than individuals 20-30 years younger, and on tests of other cognitive domains equal to or better than same-age peers [51] Age at death and postmortem interval were not different among the three groups ($p>0.05$). Please see Table S1 for characteristics of participants.

TUNEL staining of mouse brains

Brains of the indicated genotypes were harvested from mice following transcardic perfusion with 4% PFA in PBS. Harvested brains were immediately placed in 4% PFA and fixed overnight at 4°C. Brains were then briefly washed with cold PBS and transferred to 30% sucrose for cryoprotection. Brains were oriented following sagittal segmentation in OCT, sectioned, and mounted on glass slides. TUNEL staining was performed using the 594-TUNEL Assay Kit (Cell Signaling #48513) per the manufacturer's instructions. In brief, slides were rinsed in PBS to remove residual OCT medium and then permeabilized in 5% BSA/0.2% TX-100 in PBS for 30 min. Slides were washed two times in PBS then incubated for 5 min in TUNEL equilibration buffer. Next, slides were incubated for 2 hrs at 37C in TUNEL reaction mix in a humidified, dark environment. Slides were then washed 3 times in BSA/TX PBS solution above. Finally, coverslips were applied using Prolong Diamond Antifade Mountant with DAPI (Invitrogen P36931).

Slides were then imaged on a Nikon Ti-E epifluorescence microscope with Andor Clara ECCD camera and processed using Nikon Advanced Research (NIS) Elements software. Quantification of TUNEL+ cells was achieved by automatically defining and separately masking TUNEL signal and the DAPI signal using NIS Elements. TUNEL+ cells were defined where TUNEL signal was observed in the DAPI masked area using automated analysis. Automated results were subsequently verified by manual counting. TUNEL signal that was observed outside of the DAPI masked area was not included in this analysis for both automated and manual counting, although may represent additional cell death in cells that no longer stain DAPI positive.

iPSC derived excitatory forebrain neurons from an AD patient

Generation of iPSC lines from AD patients (AD1: AG5810-F [APOE3/4]; AD2: AG011414 [APOE3/4]) and healthy controls (Control 1 NUAD0635 [PBMC], Control 2: AG02261 [APOE3]) were previously described and obtained from Coriell Institute for Medical Research [52] (AG5810, AG011414, AG002261) or provided by Northwestern University's Mesulam Center for Cognitive Neurology and Alzheimer's Disease (NUAD0635). iPSCs were differentiated to forebrain excitatory neurons via lentiviral-mediated overexpression of *neurogenin-2*, as previously described [53] with minor modifications. Stem cells were maintained in mTeSR1 media (Stemcell Technologies) on Matrigel coated dishes (Corning). Upon start of differentiation, cells were single cell dissociated using Accutase (Millipore) and resuspended in mTeSR1 with 10 μM ROCK Inhibitor Y-27632 with lentiviruses encoding rrTA and pTetO-Ngn2-puro (generated by the Northwestern University Skin Biology & Diseases Resource-Based Center. The following day, medium was changed to KO-DMEM (Thermo Fisher Scientific), 1X MEM nonessential amino acids, 1X Glutamax, and 0.1% 2-mercaptoethonal, supplemented with 10 μM SB431542 (Stemgent), 100 nM LDN193189 (Stemgent), 2 μM XAV939 (Tocris Bioscience, Bristol, UK), and 3 μg/ml doxycycline (Sigma). Gradually, medium was changed over 2 days to neural induction medium, DMEM/F-12 containing MEM nonessential amino acids, Glutamax, N-2 (Thermo Fisher Scientific), D-glucose (Sigma), 2 μg/ml heparin sulfate (Sigma) supplemented with 3 μg/ml doxycycline and 2 μg/ml puromycin. Induced neurons were replated onto 6-well tissue culture plates at 450k cells/well on pre-coated with poly-L-orthnithine (Sigma), 4 μg/ml Laminin (Roche Basel, Switzerland), and 2 μg/ml Fibronectin (Sigma), cultured with neuronal maturation medium (BrainPhys Basal Medium [Stemcell Technologies], B-27 and N-2 supplements [Thermo Fisher Scientific], MEM nonessential amino acids, and Glutamax, supplemented with 3 μg/ml doxycycline and 10 ng/ml BDNF [R&D systems]). Post-plating, cells were treated with 3 μM Ara-C for 48 hrs to eliminate proliferating cells. Half of the medium was exchanged every 2 to 3 days until cell collection.

iPSC derived midbrain dopamine neurons used for *in vitro* aging study

Human iPSC from a previously characterized healthy control (line 2135 or C3 in [54]) were cultured in mTeSR1 media (Stemcell Technologies) on vitronectin coated dishes. iPSCs were dissociated into single cells by accutase treatment and seeded at 5,000 cells per cm^2 in a Matrigel coated dish. Differentiation was carried out as described [54] using dual SMAD inhibition followed by stimulation of sonic hedgehog and canonical WNT signaling. Cells were passaged en bloc at day 15 and then manually passed onto 10 cm dishes coated with poly-D-lysine at 66 μg/ml (Sigma # P1149) and laminin at 5 μg/ml (Roche # 11243217001). Cells were cultured in the presence of differentiation factors for 40 days, and then maintained in Neuraobasal media (Life Technologies) supplemented with Neurocult SM1 (Stemcell Technologies) and 1% penicillin / streptomycin (Life Technologies) until harvesting up to day 190.

To characterize iPSC derived neurons by immunocytochemistry, differentiated midbrain neurons were fixed in 4% paraformaldehyde in phosphate buffered saline (Life Technologies) for 20 min followed and permeabilized / blocked in PBS with 0.3% Triton X-100 containing 2% bovine serum albumin and 3% normal goat serum for 30 min. Primary antibodies were added and incubated overnight at 4°C in blocking buffer. Cells were then incubated in anti-mouse or rabbit IgG conjugated Alexa 488 (1:400) or Alexa 568 (1:200) (Life Technologies) for 1 hr, washed, then mounted in 10 μl of 4,6-diamidino-2-phenylindole dihydrochloride (DAPI)-containing Fluoromount G (Southern Biotech, #0100-20). Coverslips were analyzed by microscopy using a Leica confocal microscope (Leica TCS SPE laser at 25-50% power; CTR4000 / DMI4000B microscope) through a 10 μm section (z-series at 1 μm per section). The percentage of each cell population (FOXA2 / TH; LMX1A / βiiiTubulin) was quantified and normalized to total cell number through DAPI staining.

Ago pull-down and subsequent small RNA-seq (Ago-RP-Seq)

Ago pull down of the samples used in the study was performed as previously described [55]. Briefly, frozen brain pieces from human (~250 mg, frontal cortex), mouse (~150 mg, cortex and hippocampus combined) and the cell pellets obtained from iPSC derived neurons (10^6), RA/BDNF differentiated SH cells (1.5 x 10^6), NB7 parental

and Drosha k.o. clones (10^6), NB7 cells transfected with siRNAs ($1.5x10^6$) were lysed in 1 ml NP40 lysis buffer [50 mM Tris pH 7.5, 150 mM NaCl, 5 mM EDTA, 0.5% NP-40, 10% (v/v) glycerol, 1 mM NaF; supplemented with 1:200 EDTA-free protease inhibitors (Millipore #539134) and 1:1000 RNaisin Plus (Promega #N2615) before use]. For complete lysis, cells were kept on ice for 15 min, vortexed occasionally, and then centrifuged at 20,000g for 20 min. In the case of brain tissue samples, lysates were prepared by homogenizing tissues several times using Dounce Tissue Grinder in the same lysis buffer (Duran Wheaton Kimble # 357538). Pull down of Ago proteins (Ago 1-4) was performed by incubating 500 µg of Flag-GST-T6B peptide [56] (Sigma #M8823) with 80 µl of anti-Flag M2 Magnetic beads (Sigma #M8823) at 4°C for 3 hrs in a rotor. Subsequently, beads were washed three times and resuspended in 1 ml NP40 lysis buffer. To confirm pull down of Ago proteins, 50 µl aliquot containing beads were mixed with 2x SDS-PAGE sample buffer and run on 10% SDS-PAGE gel for western blot analysis by anti-Ago2 antibody. After validation, reminder of the beads was used for RNA extraction using Trizol reagent (Ambion #15596018). Subsequently RNA pellet was resuspended in 20 µl ultra-pure H_2O and 10 µl was kept for RNA visualization purposes while another 10 µl was used for small RNA library preparation using Illumina primers (RRID:SCR_010233) as described previously [57]. Briefly, RNA was ligated with 3′-adenylated adapters using T4 RNA Ligase 2 (NEB #MO351) for 4 hrs at 16°C. Product was ethanol precipitated and run on 15% Urea-PAGE gel. To determine correct position of the ligated product in the gel, radiolabeled (^{32}P) unligated and ligated size markers (19-35nt) were also run in parallel. Ligated product was then eluted from the gel and prepared for 5' adaptor ligation. Ligation of 5' adaptor to already 3' ligated RNA product was performed with T4 RNA ligase 1 (NEB, #EL0021) at 37°C for 1 h. The product was again run on 12% Urea-PAGE gel, extracted and reverse transcribed using Superscript III reverse transcriptase (Invitrogen #18080–044). Enrichment of product was performed by amplifying cDNA with multiple rounds of few cycles PCR. Quality of cDNA was validated by bioanalyzer analysis with a single peak at ~157 bp length. Sequencing of cDNA was performed on Illumina Hi-Seq 4000. The sequence information on size markers, 3' and 5' adaptors, RT primers, and PCR primers were previously published [58].

6mer seed toxicity (SPOROS) analysis

The SPOROS pipeline [35] was used to generate seed toxicity graphs, seed toxicity plots and seed nucleotide composition analyses. Briefly small RNAseq data sets in the form of raw fastq files were de-multiplexed, trimmed, cleaned and then compiled into a single read count table. After removing rare reads as described [35], the remaining reads were BLASTed against lists of small RNAs from either mouse or human. Reads that matched artificial sequences in the database were removed and final raw read count table (rawCounts) was generated. The raw read count table was used to generate two read count tables; one normalized read count table (normCounts) that contained 1 million reads per sample, and the other normalized and differentially expressed read count table (differential). After annotating each count table with 6mer seed, average 6mer seed viability, miRNA, and RNA world data, various seed toxicity analyses were done. Seed toxicity graphs were generated by adding and collapsing all rows that contained same 6mer seed and RNA type and aggregating all the read counts within that 6mer seed viability in 1% bin size. Graphs were prepared in Excel with smoothing line function on. Shown in the graphs are the peaks of normCounts plotted against % 6mer seed viability. When determining the average seed toxicity or seed composition analysis each row counts were first normalized by 1000 to ease computational complexity and the columns containing 6mer seeds and average 6mer seed viability were expanded based on the normalized read counts. Table containing frequency distribution of average 6mer viability for various groups were then used to generate basic boxplot (StatPlus (v.7.5)). Statistical analysis was done with Kruskal-Wallis test when comparing groups. Weblogo plots were generated to show average seed composition in positions 1-6. The differential expression analysis between two groups was done by taking significantly (p-value <0.05) expressed reads for each row between two groups and expressing them in delta read counts (perturbed sample-control sample). The frequency of average 6mer seed viability or 6mer seeds were then expanded based on the delta read counts to get the seed toxicity graph, seed toxicity plots, or seed toxicity compositions as described above.

Results

Evidence for a contribution of DISE to Aβ42-induced toxicity *in vitro*.

To determine whether 6mer seed toxicity could be involved in the death of brain derived cells, we chose the well characterized SH-SY5Y (SH) cell line differentiated into neurons to model neurotoxicity upon treatment with Aβ42 oligomers [59-61]. Similar to other brain-derived cell lines [32], SH cells were susceptible to siRNAs that carry toxic 6mer seeds such as an siRNAs carrying the 6mer seed of miR-34a-5p (GGCAGU) [29] or the consensus toxic seed for human cells, GGGGGC (recently identified [32]) (**Fig. 1A**). SH cells gain sensitivity to Aβ42 toxicity after differentiation [62]. We demonstrated that our preparation of Aβ42 oligomers was more active than control nonaggregating Aβ40 in SH cells fully differentiated for 7 days either by treating them with 1 mM dbcAMP [63] (**Fig. S1**) or by using a differentiation protocol involving retinoid acid (RA) and brain-derived neurotrophic factor (BDNF) [64] (**Fig. 1B**-**D**). After establishing the specific activity of Aβ42, we decided to use the more physiologically relevant protocol of differentiating SH cells with RA and BDNF for all subsequent experiments.

We recently reported that a minor shift in the loading of toxic sRNAs into the RISC can cause activation of DISE [65]. To determine whether the toxicity of Aβ42 to SH cells was associated with a shift to more toxic RISC bound reads, we treated 7-day differentiated SH cells with Aβ42 for 2, 4, and 6 hours. We chose these time points to capture changes before the initiation of cell death, which was first detectable 24 hrs after treatment (**Fig. 1D** and data not shown). R-sRNA were identified by an Ago1-4 peptide pulldown, and RNA precipitation combined with high-throughput sequencing (Ago-RP-Seq) as described [65]. Employing the SPOROS pipeline we developed to analyze RNA seq data in a seed based fashion [35] we found that the sRNAs that were significantly enriched in the RISC of cells treated with Aβ42 compared to cells treated with Aβ40 had a significantly lower seed viability than sRNAs that were depleted in the RISC (**Fig. 1E**).

We previously showed that most of the 6mer seed toxicity depends on the activity of the RISC component Ago2 [29] and that Ago2 deficient HCT116 cells are resistant to DISE induced by toxic seed containing siRNAs [65]. We used the Ago2 inhibitor aurintricarboxylic acid (ATA) [66] to test whether RISC inhibited neuron derived cells were protected from toxic RNAs that kill through Ago2 [29, 38]. We treated the neuroblastoma cell line NB7 with increasing concentrations of ATA and showed that this inhibited DISE induced by either the two toxic seed-containing siRNAs used above or by the highly toxic Huntington's disease derived CAG trinucleotide repeat containing siRNA siCAG we recently described [38] (**Fig. S2A**). ATA inhibited toxicity induced by all three siRNAs in a dose dependent manner. Undifferentiated SH cells (used because their growth could be monitored by an IncuCyte analysis) were also protected from siCAG induced cell death by ATA (**Fig. S2B**) and a rescue of siCAG induced cell death was observed in differentiated SH cells (**Fig. S2C**).

To determine whether ATA did indeed act by inhibiting Ago proteins and hence RNAi, we performed an Ago-RP-Seq analysis of NB7 cells transfected with either 1 nM siNT1, siGGGGGC or siGGGGGC in the presence of 10 μM ATA (**Fig. S2D**). siGGGGGC made up ~6% of all pulled down normalized reads and the ATA treatment reduced this amount to ~0.3% (**Fig. S2D**). Introduction of siGGGGGC into the cells had a substantial effect on the seed viability of the RISC bound sRNAs in these cells (**Fig. S2E**). The median seed viability of siGGGGGC transfected cells dropped to 5% and ATA treatment brought this back up to 68.3% consistent with siGGGGGC no longer being toxic to the cells. This analysis confirms the activity of ATA on Ago proteins and suggests that the inhibition of the RISC uptake of the toxic siRNA is what protects the cells from transfection with siGGGGGC.

After establishing that ATA could protect cells from DISE induced by a toxic siRNA, we used ATA up to a concentration of 100 μM previously shown to protect primary neurons from Aβ42 induced death [67] and similar to the effect seen with siCAG, ATA completely blocked Aβ42 induced cell death in differentiated SH cells (**Fig. 1F**). A substantial reduction of cell death was already seen at 30 μM. We previously demonstrated that death induced by toxic seed-containing siRNAs induces production of reaction oxygen species (ROS) and DNA damage [30]. We investigated whether cell death in SH cells induced by Aβ42 also caused a similar cell stress. Consistently, we detected a significant increase in ROS levels in the cells treated with Aβ42 and that resulted in elevated DNA damage as shown by a rise in γH2AX by Western blotting (**Fig. 1G** and **1H**). Furthermore, treatment with ATA prevented the Aβ42 induced DNA damage (**Fig. 1H**). Together with our data on a shift to more toxic seed containing R-sRNAs in Aβ42-treated cells, our results suggested a contribution of RNAi to Aβ42-induced cell death in neuron-like cells.

A neuroblastoma cell line with reduced levels of protective nontoxic miRNAs is hypersensitive to Aβ42 induced cell death.

We previously demonstrated that cells deficient in either Dicer or Drosha (and therefore cannot produce most canonical miRNAs), are hypersensitive to DISE inducing stimuli such as toxic siRNAs or genotoxic chemotherapeutic reagents [29, 38, 65]. We interpreted this to be caused by the cells inability to generate high levels of protective miRNAs to block RISC access by toxic sRNAs [36]. To test whether a brain-derived cell line would gain sensitivity to Aβ42 toxicity when reducing most miRNAs, we generated Drosha knockout (k.o.) NB7 cells (**Fig. 2A**). Drosha levels in two of the clones were reduced >99% resulting in about 50% reduction of RISC bound miRNAs (**Fig. 2B**) (some of which are processed in a Drosha independent fashion, i.e. miR-320) with major miRNAs substantially reduced (**Fig. 2C**). Previously, we characterized Drosha k.o. HCT116 cells and reported that in the absence of protective miRNA expression most R-sRNAs were not miRNAs. With Ago2 expression levels unaffected the median seed toxicity across these R-sRNAs was much higher than R-sRNAs in wt cells [41]. The SPOROS bioinformatics pipeline was developed to visualized these changes in total and R-sRNAs and the effect of lack of Drosha expression on seed toxicity and cell fate was quantified by producing a number of graphical outputs [35]: 1) A seed toxicity graph that plots sRNAs according to their abundance (Y axis) and seed viability (X axis), based on the average seed viability on three human cell lines (see 6merdb.org), 2) The median seed viability of all sRNAs in form of a box plot, and 3) The average nucleotide composition of the 6mer seed. Thus, to investigate the effect of lack of Drosha on these brain derived cells we sequenced both the total cellular and the R-sRNAs from the parental cells and two Drosha k.o. clones and analyzed the sequencing data with SPOROS (**Fig. S3**). Similar to the data obtained with Drosha k.o. HCT116 cells, in the two NB7 k.o. clones, many canonical miRNAs were reduced, both in the total RNA (**Fig. S3A**) and the RISC bound fraction (**Fig. S3D**) and some other sRNAs (i.e. rRNA and tRNA fragments) entered the RISC (**Fig. S3D**). This resulted in a drop in median seed viability in both k.o. clones (**Fig. S3B**, **E**) and resulted in a more C-rich average 6mer seed in the R-sRNA of the k.o. clones (**Fig. S3F**). This result is consistent with the increase in non-miRNAs entering the RISC. We recently showed that increased loading of such toxic seed containing sRNAs primes the RISC, rendering cells more susceptible to DISE [65]. Consistent with these data, we found that the two clones were indeed much more sensitive to DISE induced by siGGCAGU (**Fig. 2D**). We also found that these clones were more susceptible to H_2O_2 induced cell death (**Fig. 2E**) mimicking the response to ROS which is induced in cells treated with either Aβ42 (**Fig. 2F**) or toxic seed containing siRNAs [30].

After establishing that NB7 cells with reduced Drosha expression were hypersensitive to DISE, we tested whether the two k.o. clones were also more susceptible to cell death induced by Aβ42 than the parental cells. Parental NB7 cells were moderately sensitive to Aβ42 relative to Aβ40 (**Fig. 2G**). In contrast, both Drosha k.o. clones were more sensitive to Aβ42-induced cell death consistent with the hypothesis that DISE could contribute to this form of cell death.

Reduced seed viability of R-sRNAs in the brains of AD mouse models with signs of neurotoxicity

To test whether 6mer seed toxicity could contribute to the neurodegeneration seen in AD, we first chose the widely used AD mouse model for early-onset forms of familial (F) AD, 5XFAD [47]. 5XFAD mice with the transgene driven by the Thy-1 promotor develop cerebral amyloid plaques and gliosis at two months of age, achieve high Aβ42 burden, and have reduced synaptic markers and a late neuron loss. However, these mice do not form NFTs and do not show much of an increase in staining for p-Tau [47, 68] both key features of human AD. Finally, they also do not show a significant degree of neuronal cell death within the first few months [47]. No significant increase in TUNEL staining was found in brains of 6 or 8 months old mice (**Fig. 3A, B**). We performed an Ago-RP-Seq-SPOROS analysis of cortex and hippocampus from 6 months old 5XFAD mice. A number of miRNAs were significantly differentially expressed, most notably miR-9-5p (**Fig. 3C**). An analysis of these differentially expressed sRNAs showed that the median seed viability of all R-sRNAs was higher in the brains of 5XFAD mice compared to age-matched control mice (**Fig. 3C**) suggesting that 6mer seed toxicity was not a driver of AD symptoms in this model, at least not at 6 months, a time at which there was little detectable cell death (**Fig. 3A, B**).

Recently, a more aggressive model of AD was described based on the 5XFAD mice [48]. It was shown that LC3-associated endocytosis (LANDO) in microglia is a critical regulator of immune-mediated Aβ aggregate removal and microglial activation in the 5XFAD mice. One of the gene mutations causing LANDO deficiency that were crossed into the 5XFAD background was a deletion of Rubicon. Rubicon is a gene that constrains canonical autophagy [69]. In the absence of Rubicon 5XFAD mice developed accelerated disease pathology and neurodegeneration, reactive microgliosis, tau pathology, and behavioral impairment similar to what is seen in human AD patients. A significant difference between 5XFAD and these Rubicon k.o. mice was that they develop neuronal cell death early in the disease progression [48] (**Fig. 3A, B**). We compared the content of the RISC in mouse brains (cortex and hippocampus) of 6 months old 5XFAD Rubicon$^{-/-}$ mice with advanced disease to the

brains of three symptom-free age-matched 5XFAD Rubicon$^{+/-}$ mice. In both genotypes miRNAs constituted >96% of the R-sRNAs. Interestingly, we again observed upregulation of miR-9-5p as seen in 5XFAD mice. However, in contrast to the 5XFAD mice, the median seed viability in the 5XFAD Rubicon$^{-/-}$ mice was significantly reduced (**Fig. 3D**). This correlates with the increased Aβ42 levels in this model [48] and the resulting occurrence of cell death (**Fig. 3A, B**).

It has been shown that Aβ toxicity is dependent on the presence of Tau. Thus, hippocampal neurons obtained from tau k.o. mice did not degenerate when cultured in the presence of aggregated Aβ [70, 71]. Furthermore, tau depletion ameliorated Aβ-induced behavioral deficits when compared to transgenic mice overexpressing FAD-mutant amyloid precursor protein (54). A growing body of evidence suggests that Aβ induces a series of post-translational tau modifications including its cleavage into a neurotoxic tau$_{45-230}$ fragment. High levels of this fragment were detected in human brains obtained from AD and other tauopathy subjects [72]. In addition, transgenic mice expressing tau$_{45-230}$ under the control of the Thy 1.2 promoter showed enhanced cell death of pyramidal hippocampal neurons as early as 3 months after birth, progressive synaptic loss in the hippocampus, and behavioral deficits when compared to wild type controls [73]. We therefore subjected brains (hippocampi) from 3 months tau$_{45-230}$ transgenic mice (Tau tg) to the same analysis as the other two mouse models (**Fig. 3E**). Consistent with the increase in cell death seen in this model, the median seed viability of R-sRNAs in the brains of these mice was reduced by more than 10% (insert in **Fig. 3E**). Like in the two previous AD models miR-9-5p was again strongly enriched in the RISC in the brain of these mice compared to control mice corroborating previous findings on the role of miR-9-5p in neurodegeneration [74, 75]. A comparison of the data from all three mouse models suggested that the Ago-RP-Seq method reproducibly pulls down the same miRNAs from mouse brains. In fact, the majority of miRNAs that were found bound to the RISC in the three mouse models were shared between the models (miRNAs labeled in black in **Fig. S4**). In summary, the analysis of the R-sRNAs from the brains of three different mouse models of dementia suggest a possible contribution of 6mer seed toxicity to the neurotoxicity seen in two of the three models that show substantial neuronal cell death.

Increased seed viability of R-sRNA in Alzheimer patient brains

The data on the three AD mouse models and the *in vitro* data on SH cells suggested that a lower seed viability is associated with an increase in neurotoxicity. To determine whether this could also be found in the brains of AD patients, we compared R-sRNAs in the frontal cortex of seven postmortem AD with five control (CN = cognitive normal) brains (**Fig. 4A**, **B**, **Table S1**). The age of the brain donors ranged from 77 to 93 for the AD patients and 76 to 100 for the controls. All AD cases had "high AD neuropathologic change" [50, 76]. Neurofibrillary tangle stages of the selected AD patients were Braak 5-6 and Aβ plaque stages were all CERAD frequent. In the control cases, neurofibrillary tangles ranged from Braak stage 1-2 and Aβ plaques ranged from absent to frequent. Again >94% of all R-sRNAs were miRNAs supporting the efficiency of the pull down (**Fig. 4A**). Surprisingly, AD brain RISCs were enriched in R-sRNAs with higher seed viabilities than control brains (**Fig. 4B**). To confirm this observation, we repeated the entire library preparation and sequencing of R-sRNAs using the same Ago associated RNA previously isolated from the same brains (**Fig. S5A**). The nature of the pulled down sRNAs was very similar in both experiments (**Fig. S5B**). Consistent with the previous analysis we found significantly higher seed viability of R-sRNAs in AD brains than in the control brains (**Fig. S5A**, right panel). This was further confirmed by isolating fresh RNA from a pair of three AD and three control brains (**Fig. S5C**). While in all analyses of mouse and human AD we saw an increase in miR-9-5p, and in the human brains of miR-21-5p, the data on seed toxicity in human AD brains seemed to contradict the results obtained with two of the mouse models that showed signs of neuronal death. One interpretation of the data is that reduced seed viability of R-sRNA may only be found in a situation of ongoing neuronal loss. It is important to consider that AD develops in humans over many years and that brain regions and neurons have different vulnerabilities to neurodegeneration [77]. Brains from human AD patients which can only be collected postmortem may only contain neurons from brain regions that were relatively resistant to the toxic environment and may have survived because they have sRNAs bound to their RISC with higher seed viability.

To test this hypothesis, we analyzed iPSC derived neurons generated from two control and two AD patients (**Fig. S6A**, **B**). AD derived iPSC neurons had highly upregulated Tau1 protein and showed signs of ongoing DNA damage stress with increased H2AX phosphorylation (**Fig. S6C**). The overall nature of the R-sRNAs in these iPSC derived neurons (**Fig. S6D**) was similar to the one we detected in the RISC of actual human brains (**Fig. 4A**) consistent with the neuronal nature of these cells. Interestingly, the seed viability of sRNAs bound to the RISC of AD iPSC derived neurons was significantly lower than the ones bound to the RISC of control cells (**Fig. S6E**) suggesting that in cells from AD patients toxic R-sRNAs may indeed predominate.

Finally, we tested how an extended treatment of neuronal cells with Aβ42 would affect the composition of the RISC in an attempt to emulate the conditions that neurons in AD patients may be encountering. When differentiated SH cells were treated with Aβ42 for 6 hours, as expected, the median seed viability of R-sRNAs dropped (**Fig. 4C**, left panel). In contrast, when the cells were treated for 48 hrs, a time point at which a substantial number of cells had already died, we detected an increase in median seed viability of R-sRNAs in the surviving cells (**Fig. 4C**, right panel) suggesting that chronic exposure may result in the induction of a protective response or the selection of cells with higher resistance. Interestingly, when we compared the pulled down miRNAs in seed toxicity graphs we found that only in 48 hr stimulated cells miR-21-5p was significantly upregulated (**Fig. 4C**, right panel). This parallels the observation that miR-21-5p was upregulated in the RISC of AD brains and is consistent with the reported protective role of this miRNA in many brain disorders, particularly in AD [78].

We detected specific changes in both brains from human AD patients and from mouse models of AD that suggest that 6mer seed toxicity may contribute to cell death of neurons. We do not believe that the observed difference between normal and AD brains is due to an increase in infiltrating immune cells because an analysis of neuron, glia and macrophage/lymphocyte specific miRNAs [79-82] bound to the RISC did not support that interpretation (**Fig. S7**). In summary, the data suggest that 6mer seed toxicity may contribute to neuronal cell death in mouse models of AD, and in the brains of human AD patients. Neurons surviving after years of disease progression may be enriched in protective miRNAs, suggesting that brain cells with toxic sRNA in the RISC that are more toxic are lost earlier during the course of the disease.

6mer seed toxicity and AD during aging

miRNAs have been shown to protect neurons from cell death [83, 84], but aging neurons may be less able to generate miRNAs [85]. Such aging neurons could be more susceptible to small RNAi active RNAs that induce cell death. To test whether aging neurons would lose their protection by nontoxic miRNAs, we compared the RISC content of the brain cells of young (2 month old) with that of old (18 month old) mice (**Fig. 5A**). We found that the RISC in brain cells (cortex and hippocampus) of older mice contained significantly more sRNAs with low seed viability suggesting that they may be less able to protect themself against the activity of toxic sRNAs. This was independently confirmed in an analysis of another set of young and old mice (**Fig. S8A-E**). The miRNAs that were pulled down in these two experiments were very similar (shown in black in **Fig. S8A**), median seed viabilities of all R-sRNAs in these samples were identical (**Fig. S8C, D**), and a Pearson correlation demonstrated high reproducibility between the two experiments (**Fig. S8E**). Just like in experiment #1 in experiment #2 the median seed viability of the differentially expressed R-sRNA was lower in the brains of old versus young mice (**Fig. S8F**).

How could aging neurons lose their protection by nontoxic miRNAs? A progressive loss of Dicer and the resultant global decrease in miRNA expression with age has been suggested as one mechanism. A study showed that Dicer expression in the brains of two year old mice is substantially reduced compared to the brains of 6 week old mice [85]. We therefore wondered whether neurons with increasing age would lose expression of some of their protective miRNAs and whether sRNAs that are enriched in older neurons could be more toxic, rendering the neurons primed for DISE.

To test whether the loss of protective R-sRNAs can be seen in aged neurons *in vitro,* we tested iPSC derived neurons that were aged in a dish [86] (**Fig. S9**). These cells were cultured for up to 190 days in poly-d-lysine and laminin coated dishes. We detected a substantial loss of Dicer protein with increasing age (right insert in **Fig. 5B**). An Ago-RP-Seq-SPOROS experiment confirmed a significant decrease in seed viability of even total R-sRNAs in the five month old versus one month old iPSC derived neurons (left insert in **Fig. 5B**).

While an analysis of brain cells from young and older individuals is not feasible, it was shown before that besides the brain another tissue whose miRNA content changes with age is spleen/immune cells [85]. Consistently, another study had reported major changes in the miRNA content of peripheral blood mononuclear cells (PBMCs) between young and old cohorts [87]. A reanalysis of these data for the seed viability of the differentially expressed mature miRNAs revealed a substantial drop in median seed viability in the miRNAs upregulated in the PBMCs from the old cohort (**Fig. 5C**). This is line with our data on the mouse brains and suggests that with age different tissues may be more primed to die by DISE.

If the assumption is correct that a lower seed viability of R-sRNAs in brain cells contributes to neuronal death and dementia, then individuals that manage to maintain a high level of protective miRNAs in the RISC would be less prone to AD or other forms of dementia. To test this hypothesis, we analyzed the RISC content of brain cells from SuperAgers which are individuals age 80 and above whose episodic memory performance is at least at the level of cognitively average individuals in their 50s and 60s [51]. We obtained brain tissue from three SuperAgers and compared them to three of our CNs of a similar age. We did indeed find that the RISC in the SuperAger

brains (average age = 90 years) contained sRNAs with a significantly higher seed viability than in control brains (average age 85.7 years) (**Fig. 5D**, **E** and **Fig. S10A, B**) or even the AD brains (**Fig. S10C**). These preliminary data suggest that SuperAgers have a greater resilience to the damage by toxic sRNAs which may contribute to dementia such as AD. In summary, our data are consistent with DISE contributing to the etiology of AD. Aging neurons may be more prone to this form of cell death but individuals that can maintain higher seed viability of their R-sRNAs are more resilient to AD.

Discussion

We discovered DISE/6mer seed toxicity as a powerful anticancer mechanism and predicted that it may have implications for other diseases [36]. Interestingly, it has been reported that AD patients are less prone to getting cancer and cancer patients in general show lower AD incidence [88, 89]. This was the original motivation to test for a potential role of DISE in the etiology of AD. Our analysis of R-sRNAs in various AD models supports DISE/6mer seed toxicity as a new concept of cell fate regulation that may affect the survival of neurons. We found a significant correlation between the level of neurotoxicity and the seed viability of R-sRNAs, and inhibiting RISC loading protected neuronal cells from the toxicity of Aβ42. Lower seed viability correlated with higher levels of cell death. Correspondingly, a higher overall seed viability of the RISC content may protect neurons from dying. The RISC in postmortem AD brains contained R-sRNAs with higher seed viability possibly due to a selection for more DISE resistant cells during the disease, consistent with the analysis of SH cells that had survived a 48 hr treatment with Aβ42. Seed viability was lower in older mouse brains and in *in vitro* aged iPSC derived neurons suggesting a loss of protective miRNAs with age. In contrast, the RISC in brain cells from SuperAgers contained significantly greater amounts of sRNAs with higher seed viability suggesting a higher resilience of these individuals against neuronal loss caused by DISE.

While our analysis included any sRNA that can enter the RISC, in most cells including neurons >95% of the RISC content are miRNAs. The role of miRNAs in AD has been intensively studied ([90, 91]). Most analyses on AD associated miRNAs are based on quantifying miRNAs from total small RNA fraction and different miRNAs have been associated with the disease [90, 91]). We recently analyzed short RNAs in total RNA from a large cohort of AD patients [35]. Our data suggested that a substantial number of sRNAs other than miRNAs were upregulated in AD patient brains compared to controls. However, we and others have found that miRNAs vary dramatically in their ability to be taken up by the RISC [65, 92]. We therefore decided to subject various *in vitro* and *in vivo* systems as well as patient samples to an analysis of RISC bound short RNAs. We chose an Ago-RP-Seq method rather than a method involving cross-linking miRNAs with their targets, as we were not per se interested in identifying miRNA targets. We provide data on 6mer seed toxicity contributing to the neurotoxicity seen in AD.

Based on our data we are now proposing a new mechanism that may explain the tissue loss seen late during the progression of AD: An age dependent imbalance between sRNAs that are toxic to neurons through RNAi and miRNAs that contain nontoxic seeds and act as protectors from 6mer seed toxicity. We are proposing that miRNAs play at least two fundamental roles in most tissues: First, they regulate multiple pathways by targeting hundreds of genes, mostly involved in development and differentiation. Second, they are expressed at high levels preventing access of toxic sRNAs to the RISC.

There is ample literature to support the notion that miRNAs are neuroprotective in a number of diseases and disease models: In *Drosophila* impairing miRNA processing dramatically enhanced neurodegeneration caused by the CAG repeat gene ATXN3 [93]. We previously demonstrated how toxic CAG repeat-derived siRNAs cause cell death [38]. Consistently, pathogenic ATXN3 with amplified CAG repeats showed strongly enhanced toxicity in HeLa cells after knockdown of Dicer [94]. Multiple publications on mice with a tissue specific knock-out of Dicer in brain cells showed that reducing Dicer triggers neuronal loss and causes behavioral abnormalities, followed by the premature death of the animals (see e.g. [83, 84]). Moreover, mice with a tissue specific deletion of Dicer in spinal motor neurons exhibit hallmarks of spinal muscular atrophy (SMA) with signs of denervation [95]. Interestingly, mice with a brain specific knock out of Ago2 (using the same promoter: CaMKII Cre) showed no toxicity in neurons [96] suggesting that it is not the general activity of miRNAs and RNAi that is required for survival of neurons. Conversely, increasing miRNAs levels can be neuroprotective. Amyotrophic Lateral Sclerosis (ALS) disease mice treated with the antibiotic Enoxacin [97], which causes a global upregulation of miRNAs by stabilizing Dicer/TRBP [98, 99], showed reduced disease scores [100]. In addition, it was directly shown that miRNAs in Dicer knockout mice protect adult dopamine neurons from neurotoxicity [101] and Enoxacin treatment promoted survival of cultured DA neurons.

It was previously reported that the brain is one of three tissues that lose most of its Dicer and consequently its miRNA expression with age [85]. It is therefore possible that neurons when they age gradually lose expression of protective miRNAs rendering them susceptible to RNAi based toxicity. This toxicity could be at the core of many degenerative diseases that affect the brain, among them AD, Parkinson's disease (PD), Huntington's disease (HD), and ALS. As this loss in humans likely occurs over decades, this would explain why so many neurodegenerative diseases have an onset during adulthood with decades of symptom-free life. Based on our data we are now proposing a new model to explain AD etiology with implications for other neurodegenerative diseases. This model focuses on RNAi and the RISC complex as a central rheostat in all cells that when thrown out of balance results in cell death: Any 19-25 nt long sRNA when loaded into the RISC carrying a toxic 6mer seed can kill cells through DISE/6mer seed Tox [29, 31, 39, 41, 102] (**Fig. 6a**). Aβ oligomers (AβOs) and p-Tau can elicit a cellular response that causes upregulation of endogenous toxic sRNAs (**Fig. 6b**). Normal cells and neurons in younger individuals are protected by expressing large quantities of miRNAs [83, 84] that carry nontoxic 6mer seeds (**Fig. 6c**). However, during aging mitochondria become dysfunctional resulting in an increase in the production of ROS (**Fig. 6d**). The stability of Dicer which is critical to miRNA expression in the brain [83, 84, 103, 104] is sensitive to ROS and interferons (IFNs) [105, 106] and most of its expression in the brain is lost during aging [85]. During AD Aβ plaques cause further upregulation of ROS and induce inflammation resulting in elevated IFNs (**Fig. 6d**). This results in a vicious cycle of increasing amounts of toxic sRNAs and the progressive loss of protective miRNAs resulting in synaptic loss, neuronal dysfunction, cell death, and neurodegeneration. An age dependent loss of protective miRNAs together with the upregulation or the presence of toxic sRNAs combined with numerous genetic modifiers and genetic mutations present in familial and sporadic AD may contribute to AD.

While cell death is a component of AD, it is thought to be a relatively late event in the collection of cascades that ultimately result in symptoms. That is why many in the field do not consider cell death as being essential. However, while many other manifestations of the disease such as synaptic loss are detected much earlier, the path to various pathologies that end with cell death often goes through stages of stress and cellular dysfunction such as cell cycle effects. Such a gradual effect during DISE can be seen in cancer cells. Before the cells die they slowdown in growth and display various cell cycle defects [30]. In a large and unique cell type such as a post-mitotic neuron, the disease can even affect cellular substructures as shown for developing axons due to a local activation of the RNAi machinery [107]. When patients die they have lost a substantial amount of their brain cells and it may therefore be beneficial to prevent the neurotoxicity.

Conclusions

The overwhelming investment in AD drug discovery has been focused on two mechanisms: 1) Reducing amyloid plaque load in the brain (the hallmark of AD diagnosis; 70-80% of the effort) and 2) preventing tau phosphorylation. However, treatments aimed at reducing amyloid plaque burden have not yet resulted in an effective treatment of AD (summarized in [108]). Our data support a hypothesis that high expression of nontoxic miRNAs protects from neurodegeneration and that increasing miRNA biogenesis with drugs similar to Enoxacin [99] or blocking toxic R-sRNAs may be a viable treatment option for many neurodegenerative diseases including AD.

Abbreviations

3'UTR: 3' untranslated region; Aβ: Amyloid-β; Ab42: 1-42 Aβ peptide; AD: Ago: Argonaute; Ago-RP-Seq: Ago RNA precipitation combined with small RNAseq; Alzheimer's disease; ATA: aurintricarboxylic acid; BDNF: neurotrophic factor; CN: cognitive normal; DISE: death induced by survival gene elimination; FAD: familial form of AD; iPSC: Induced pluripotent stem cells; k.o.: knockout; NFT: neurofibrillary tangles; p-tau: phosphorylated tau; RA: retinoid acid; RISC: RNA induced silencing complex; RNAi: RNA interferences; SA: SuperAger; SH: SH-SY5Y cells; sRNA: short RNA; R-sRNA: RISC bound sRNA; siRNA: Small interfering RNA; miRNA: microRNA; TNR: trinucleotide repeat; wt: Wild-type.

Supplementary Information

The online version contains supplementary material available at

Acknowledgements

We would like to thank Drs. William Klein and Ruth Itzhaki for helpful discussions and input early in the project.

Author's contributions

MP designed experiments, analyzed data, and conceptualized the work. BP designed, performed, and analyzed most of the *in vitro* experiments and BP and S-YJ performed the Ago-RP-Seq experiments. C-PM and AR stained and imaged mouse brains. AHL generated and characterized the Drosha k.o. NB7 cells. EB developed SPOROS and EB and BP performed bioinformatics analyses. KF and AF generated and cultured human iPSC derived neurons. JK and JM provided iPSC-derived neurons and their characterizing data. AM provided conceptual input. ER and CG provided the CN, AD and SuperAger brain samples. AF provided brains from tau transgenic mice. BH and DG provided the brains of 5XFAD and 5XFAD Rubicon k.o. mice and BH performed the TUNEL staining of these brains. KS and RV provided training and input on working with AD brains. MP and BP wrote, and RV, AHK, BP, and MP edited the manuscript. All authors read and approved the final manuscript.

Funding

This work was supported by National Institutes of Health grants RO1NS090993 (to A.F.), R01 AG030142 (to R.V.), R01AG045571, R56AG045571, R01AG067781, U19AG073153, P30AG072977, P30AG13854 (to R.G and C.G.), R01 NS124783, and L40CA231423 (to B.L.H). The content is solely the responsibility of the authors and does not necessarily represent the official views of the National Institutes of Health. Further support was provided by the McKnight Brain Research Foundation (to E.R.).

Availability of data and materials

RNA seq data were deposited at GEO under accession numbers GRExxxxx. All other data generated and analyzed during this study are included in this published article and its supplementary information files.

Declarations

Ethics approval and consent to participate

All animal experiments were approved and conducted in accordance with IACUC regulations at Northwestern University, St. Jude's Children's Hospital and University of South Florida, Tampa. Written informed consents were obtained from all human participants and the study was approved by the Northwestern University Institutional Review Board and in accordance with the Helsinki Declaration.

Consent for publication

Not applicable.

Competing interests

The authors declare that they have no competing interests.

Author details

[1]Department of Medicine/Division Hematology/Oncology, [3]Department of Biochemistry and Molecular Genetics, [4]Department of Preventive Medicine/Division of Biostatistics, [5]Davee Department of Neurology, [6]Mesulam Center for Cognitive Neurology and Alzheimer's Disease, [7]Department of Psychiatry and Behavioral Sciences, [8]Department of Cell and Developmental Biology, Feinberg School of Medicine, Northwestern University, Chicago, IL, [2]USF Health Byrd Alzheimer's Center and Neuroscience Institute; Department of Molecular Medicine, Morsani College of Medicine, Tampa, FL, [9]Department of Immunology, St. Jude Children's Research Hospital, Memphis, TN

[11]Current address: Ministry of Food and Drug Safety, Pharmaceutical Safety Bureau, Pharmaceutical Policy Division 187, Osongsaengmyeong 2-ro, Osong-eup, Heungdeok-gu, Cheongju-si, Chungcheongbuk-do, Republic of Korea

Figure legends

Fig. 1 Aβ42 is toxic to differentiated SH cells through 6mer seed toxicity. **A** Change in confluence over time of SH cells treated with lipid only or transfected with 10 nM of the indicated siRNA. Data points are from triplicates and mean -/+ SE. **B** Phase contrast image of undifferentiated SH cells or SH cells differentiated with RA/BDNF for 7 days. Size bar = 60 μm. **C** Western blot analysis of cells in B. **D** Viability of undifferentiated or 7 day differentiated SH cells treated with either Aβ40 or Aβ42 for 24 or 48 hrs. Data were normalized to the 24 hr treatment with Aβ40. **E** Difference in seed viability of R-sRNAs significantly ($p<0.05$) under- or overrepresented in 7 day differentiated SH cells treated with Aβ42 for different periods of times (compared to Aβ40 treated cells). Shown are the medians and Kruskal-Wallis median test p-values. **F** Viability assay of differentiated SH cells treated for 72 hrs with either 10 μM Aβ40 or Aβ40 in the absence or presence of different concentrations of ATA. **G** Quantification of ROS levels in differentiated SH cells treated with either Aβ40 or Aβ42. **H** Western blot for γH2AX of 7 day differentiated SH cells treated with Aβ40 or Aβ42 for four hours in the absence or presence of 100 μM ATA. Shown are data from triplicates with SD and Student's ttest p-value (D, F, G).

Fig. 2 Drosha k.o. NB7 cells are hypersensitive to toxicity of Aβ42. **A** Western blot analysis of parental NB7 cells and two Drosha k.o. clones. Densitometrical quantification of Drosha relative to Actin is shown. Par, parental. **B** Relative amounts of total RISC bound miRNAs of the cells in A. **C** Real-time PCR quantification of major miRNAs in the two k.o. clones relative to parental cells. Shown are averages with variance of samples done in duplicate (miR-221/miR-181) or SD of samples done in triplicate (Let-7a and miR-21). The data on miR-21 and Let-7a are representative of two biological replicates. **D** Change in confluence over time of NB7 parental cells or two Drosha k.o. clones treated with lipid only or transfected with 1 nM of siGGCAGU. Data points are from triplicates and mean -/+ SE. **E** Viability assay of parental and two Drosha k.o. clones 24 hrs after a 3 hr treatment with 25 or 50 μM H_2O_2. **F** Quantification of ROS levels of NB7 cells left untreated or treated with Aβ40 or Aβ42. **G** Viability assay of parental NB7 cells or two Drosha k.o. clones after a 48 hr treatment with Aβ40 or Aβ42. Mean a SD are shown (C, E, F, G) and Student's t-test p-values are shown.

Fig. 3 Reduction in seed viability of R-sRNAs in AD mouse models with neurotoxicity. **A** Representative TUNEL staining of brains of 6 months old control ($5XFAD^{Neg}$/$Rubicon^{+/-}$ and $5XFAD^{Neg}$/$Rubicon^{-/-}$), 5XFAD tg ($5XFAD^{TG}$/$Rubicon^{+/-}$), and $5XFAD^{TG}$/$Rubicon^{-/-}$ mice. Brain sections were counterstained with DAPI. Size marker = 200 μm. **B** Quantification of TUNEL positivity in brains of mice with four different genotypes. *Top,* 6-months and *bottom*, 8-months old mice. Student's T-test p-values are given. ns, not significant. **C**, **D**, **E** Seed toxicity graphs of differentially expressed R-sRNAs ($p<0.05$) between Ctr and 5XFAD (C), 5XFAD $Rubicon^{+/-}$ (Het) and 5XFAD $Rubicon^{-/-}$ (D), control and Tau tg (E) brains. miRNAs are labeled that have a difference in expression of 1000 or more reads. Enriched sRNAs are shown in green and depleted sRNAs in red. Shown are averages of triplicate (C, E) or quadruplicate (D) samples. Inserts: Seed toxicity plots of the seed viability of the same samples. Medians and Kruskal-Wallis median test p-value are given.

Fig. 4 Increased seed viability of R-sRNA in postmortem human Alzheimer patient brains and differentiated SH cells treated with Aβ42 for 2 days. **A**, **B** Seed toxicity graphs of total R-sRNAs (A) and differentially expressed R-sRNAs (B) of CN and AD brains. Shown are averages of 5 (CN) and 7 (AD) samples (experiment #1). **C** Seed toxicity graphs of differentially expressed R-sRNAs of 7 day differentiated SH cells treated with either Aβ40 or Aβ42 for 6 hrs (left) or 48 hrs (right). Shown are averages of 2 samples. sRNAs with 10s000 or more reads in at least two samples (A) or that have a difference in expression of 1000 or more reads (B, C) are labeled. In each label sRNAs are listed in the order of expression levels. Enriched sRNAs are shown in green and depleted sRNAs in red. Inserts: Seed toxicity plots of the differential seed viability of each analysis. Medians and Kruskal-Wallis median test p-value are given.

Fig. 5 Changes in seed viability of R-sRNAs with age. **A** Seed toxicity graph of differentially expressed R-sRNAs of 2 months and 18 months old mouse brains. Shown are averages of triplicate samples. sRNAs that have a difference in expression of 1000 or more reads are labeled. Enriched sRNAs are shown in green and depleted sRNAs in red. Insert: Seed toxicity plot of the differential seed viability of the analysis. Medians and Kruskal-Wallis median test p-value are given. **B** Seed toxicity graph of total R-sRNAs of iPSC derived neurons aged for 1 and 5 months. sRNAs with 10,000 or more reads in at least one sample are labeled. In each label sRNAs are listed in the order of expression levels. Enriched sRNAs are shown in green and depleted sRNAs in red. Insert: Seed toxicity plot of the differential seed viability of the analysis. Medians and Kruskal-Wallis median test p-value

are given. Western blot insert: Analysis of iPSC derived neurons aged *in vitro* for 30, 150 or 190 days. Densitometrical quantification relative to the 30-day time point and actin is given. **C** *Top*, Average seed toxicity of all significantly up- and downregulated miRNAs in PBMCs of old versus young donors [87]. *Bottom*, Nucleotide composition at each of the six seed positions in the miRNAs analyzed above. **D** Seed toxicity graph of differentially expressed R-sRNAs of postmortem CN and SuperAger brains. Shown are averages of triplicate samples. sRNAs that have a difference in expression of 1000 or more reads are labeled. In each label sRNAs are listed in the order of expression levels. Enriched sRNAs are shown in green and depleted sRNAs in red. Age of the three CN participants: 100, 87, 83 - average = 90, age of the three SuperAgers: 82, 85, 90 - average = 85.7. **E** *Top*, Seed toxicity plots of the differential seed viability of the samples in D. Medians and Kruskal-Wallis median test p-value are given. *Bottom*, average seed composition of the sRNAs in the same samples.

Fig. 6 A model on the role of 6mer seed toxicity. **a** The executioner: The RISC with bound sRNAs carrying toxic 6mer seeds causing induction of DISE. **b** The killers: Stimuli that cause the increase in toxic sRNAs in neurons above the level that the protectors can buffer. **c** The protectors: A miRNA-based mechanism that protects normal neurons from toxic sRNAs by blocking their access to the RISC. **d** The modifiers: Stimuli that cause the loss of protection of neurons and during stress and aging exposing cells to the toxic sRNAs. RISC, RNA-induced silencing complex; DISE, death induced by survival gene elimination; sRNA; short RNA; IFN, proinflammatory cytokines including interferons; AGOs, Argonaute proteins, critical components of the RISC; ROS, reactive oxygen species. Two inhibitors and their site of action are shown. Green line, neuron plasma membrane; blue line, neuron nucleus.

Supplementary figure legends

Additional file 1: Fig. S1. dbcAMP differentiated SH cells are sensitive to the toxicity of Aβ42. **(A)** Western blot analysis of SH cells cultured in DMEM or in NB-active medium with and without dbcAMP. TH, tyrosine hydroxylase. **(B)** Viability assay of dbcAMP day 1 or day 7 differentiated SH cells left untreated or treated with either Aβ40 or Aβ42 for 48 hrs. Data are in triplicate. Shown is the mean with SD and Student's t-test p-values.

Additional file 2: Fig. S2: ATA blocks RISC uptake of DISE-inducing sRNAs and protects from DISE in NB7 and SH cells. **(A)** Change in confluence over time of NB7 cells treated with lipid only or transfected with the indicated siRNA in the absence or presence of increasing concentrations of ATA. Data points are from triplicates and mean -/+ SE. **(B)** Change in confluence over time of SH cells treated with lipid only or transfected with 5 nM of siCAG in the absence or presence of 5 μM ATA. Data points are from triplicates and mean -/+ SE. **(C)** Viability assay of differentiated SH cells 72 hrs after treatment with either lipid or 5 nM of siNT1 or siCAG in the absence of presence of 10 μM ATA. Student's ttest p-value is shown for the comparison between cells treated with siNT1 versus siCAG. **(D)** Counts (normalized to 1 million reads) of the siGGGGGC antisense strand in the RISC of NB7 cells transfected with either 1 nM siNT1, siGGGGGC or siGGGGGC and treated with 10 μM ATA. Shown are the averages of biological triplicates -/+ SD. The percent of the siRNA in the total R-sRNA is given for the siGGGGGC transfected cells. **(E)** Seed toxicity plots with the seed viability of the differentially expressed R-sRNAs of the samples in C. *Left:* comparison of the reads in siNT1 and siGGGGGC transfected cells; *right:* comparison of the reads in siGGGGGC transfected cells minus/plus ATA. Shown are the medians and Kruskal-Wallis median test p-value between indicated samples.

Additional file 3: Fig. S3: SPOROS analysis of total and RISC bound sRNAs in Drosha k.o. NB7 cells. **(A)** Seed toxicity graph of all sRNAs sequenced in parental NB7 cells and two Drosha k.o. clones. sRNAs with 10,000 or more reads in at least one sample are labeled. Enriched sRNAs are shown in green and depleted sRNAs in red. **(B)** Seed toxicity plots of the seed viability of the samples in A. Shown are the medians and Kruskal-Wallis median test p-value. **(C)** Average seed composition of all sRNAs in the three samples in A. **(D)** Seed toxicity graph of all R-sRNAs sequenced in parental NB7 cells and two Drosha k.o. clones. sRNAs with 10,000 or more reads in at least one sample are labeled. Enriched sRNAs are shown in green and depleted sRNAs in red. **(E)** Seed toxicity plots of the seed viability of the samples in D. Shown are the medians and Kruskal-Wallis median test p-value. **(F)** Average seed composition of all sRNAs in the three samples in D.

Additional file 4: Fig. S4: SPOROS analysis of total sRNAs in three AD mouse models. **(A, C, E)** Seed toxicity graph of total R-sRNAs of Ctr and 5XFAD (A), 5XFAD Rubicon$^{+/-}$ and 5XFAD Rubicon$^{-/-}$ (C) and Ctr and Tau tg (E) brains. Shown are averages of triplicate (A and E) and quadruplicate (C) samples. In all cases sRNAs with

10,000 or more reads in at least one sample are labeled. In each label sRNAs are listed in the order of expression levels. sRNAs shared in all three analyses are shown in black. **(B, D, F)** *Top*, Seed toxicity plots of the total seed viability of the samples in A, C and E. Medians and Kruskal-Wallis median test p-value are given. *Bottom*, average seed composition of the sRNAs in the same samples.

Additional file 5: Fig. S5: Repeat analyses of human postmortem AD brains using SPOROS. **(A)** *Left:* Seed toxicity graph of differentially expressed R-sRNAs of CN and AD brains. Shown are averages of 5 (CN) and 7 (AD) samples (experiment #2). Enriched sRNAs are shown in green and depleted sRNAs in red. sRNAs that have a difference in expression of 1000 or more reads are labeled and in each label sRNAs are listed in the order of expression levels. *Right:* Seed toxicity plot of the differential seed viability of the analysis. Medians and Kruskal-Wallis median test p-value are given. **(B)** Pearson correlation analyses of gene products covered by the reads immunoprecipitated in the experiments shown in Fig. 4A (Exp #1) and in Fig. S5A (Exp #2). Only genes were included with an average of 10 reads across all samples. **(C)** Seed toxicity graphs of differentially expressed R-sRNAs (A) of 3 CN and 3 AD brains. Medians and Kruskal-Wallis median test p-value are given.

Additional file 6: Fig. S6: Reduced seed viability of R-sRNAs in iPSC derived neurons from AD patients. **(A)** Bright field image of the NGN2 excitatory neurons derived from two control and two AD patients 36 days post differentiation. Size bar = 500 μm. **(B)** Immunofluorescence images of the AD derived neurons using the neuronal marker βiiiTubulin and the glutamatergic neuronal marker vesicular glutamate transporter (vGLUT) counterstained with DAPI. Size bar = 50 μm. **(C)** Western blot analysis of Ctr (NUAD0635) and AD (AG5810) iPSC derived neurons. The analysis was done with half of the cells that were subjected to the Ago-RP-Seq-SPOROS analysis. **(D)** Seed toxicity graph of total R-sRNAs of the two Ctr and two AD patient derived iPSC derived neurons (average for each set is shown). Shown are averages of duplicate samples. sRNAs with 10,000 or more reads in at least one sample are labeled. In each label sRNAs are listed in the order of expression levels. **(E)** *Top*, Seed toxicity plot of the differential seed viability of the samples in A. Medians and Kruskal-Wallis median test p-value are given. *Bottom*, average seed composition of the sRNAs in the same samples.

Additional file 7: Fig. S7: Total read numbers of neuron, glia and immune cell specific RISC bound miRNAs in different brain samples. Normalized expression levels of miRNAs pulled down in different tissues in the three experiments described in Fig. 4A, 3D, and 3E. Shown are averages with SD. None of the comparisons between ctr and respective AD model reached statistical significance.

Additional file 8: Fig. S8: Repeat analysis of young and old mouse brains using SPOROS. **(A, B)** Seed toxicity graph of total R-sRNAs of 2 months and 18 months old mouse brains. Experiment #1 (A) and Experiment #2 (B). Shown are averages of triplicate (A) and duplicate (B) samples. In all cases sRNAs with 10000 or more reads in at least one sample are labeled. In each label sRNAs are listed in the order of expression levels. sRNAs shared in all three analyses are shown in black. **(C, D)** *Top*, Seed toxicity plots of the total seed viability of the samples in A and B. Medians and Kruskal-Wallis median test p-value are given. *Bottom*, average seed composition of the sRNAs in the same samples. **(E)** Pearson correlation analysis of gene products covered by the reads precipitated in the experiments shown in A (Exp #1) and in B (Exp #2). Only genes were included with an average of 10 reads across all samples. **(F)** Seed toxicity plot of differentially expressed R-sRNAs of 2 months and 18 months old mouse brains (Exp. #2). Medians and Kruskal-Wallis median test p-value are given.

Additional file 9: Fig. S9: Characterization of human iPSC-derived midbrain dopamine neurons that were aged *in vitro*. **(A)** Brightfield image of iPSCs before differentiation (day 0). **(B)** Immunostaining analysis of midbrain dopamine (DA) neurons at day 75 using antibodies that detect neuronal (βiii Tubulin) or DAergic specific markers (LMX1A, FOXA2, Tyrosine Hydroxylase (TH). DAPI (Blue) was used to stain nuclei. **(C)** Western blot analysis of DAergic markers TH, βiiiTubulin. Non-neuronal GAPDH was used as loading control. **(D)** Western blot analysis of βiiiTubulin normalized to GAPDH, quantified on the right documents the stability on the culture system over time.

Additional file 10: Fig. S10: SPOROS analysis of all R-sRNAs in brains of SuperAgers. **(A)** Seed toxicity graph of total R-sRNAs of postmortem CN and SuperAger brains. Shown are averages of triplicate samples. In all cases sRNAs with 10,000 or more reads in at least one sample are labeled. In each label sRNAs are listed in the order of expression levels. **(B)** *Top*, Seed toxicity plots of the total seed viability of the samples in A. *Bottom*, average seed composition of the sRNAs in the same samples. Medians and Kruskal-Wallis median test p-value

are given. **(C)** Seed toxicity plots of differential seed viability of postmortem SuperAger versus AD brains. Medians and Kruskal-Wallis median test p-value are given.

Additional file 11: Table S1. Description of all patient brain material used.

References

1. Prince M, Albanese E, Guerchet M, Priva M: **World Alzheimer Report 2014: Dementia and Risk** Reduction an Analysis of Protective and Modifiable Factors. *Alzheimer's Dis Int* 2014.
2. Lane CA, Hardy J, Schott JM: Alzheimer's disease. *Eur J Neurol* 2018, 25:59-70.
3. Hardy JA, Higgins GA: Alzheimer's disease: the amyloid cascade hypothesis. *Science* 1992, 256:184-185.
4. Lee VM, Goedert M, Trojanowski JQ: Neurodegenerative tauopathies. *Annu Rev Neurosci* 2001, 24:1121-1159.
5. Heppner FL, Ransohoff RM, Becher B: Immune attack: the role of inflammation in Alzheimer disease. *Nat Rev Neurosci* 2015, 16:358-372.
6. Bhat AH, Dar KB, Anees S, Zargar MA, Masood A, Sofi MA, Ganie SA: Oxidative stress, mitochondrial dysfunction and neurodegenerative diseases; a mechanistic insight. *Biomed Pharmacother* 2015, 74:101-110.
7. Dawson TM, Dawson VL: Mitochondrial Mechanisms of Neuronal Cell Death: Potential Therapeutics. *Annu Rev Pharmacol Toxicol* 2017, 57:437-454.
8. Zott B, Busche MA, Sperling RA, Konnerth A: What Happens with the Circuit in Alzheimer's Disease in Mice and Humans? *Annu Rev Neurosci* 2018, 41:277-297.
9. Niikura T, Tajima H, Kita Y: Neuronal cell death in Alzheimer's disease and a neuroprotective factor, humanin. *Curr Neuropharmacol* 2006, 4:139-147.
10. Varadarajan S, Kanski J, Aksenova M, Lauderback C, Butterfield DA: Different mechanisms of oxidative stress and neurotoxicity for Alzheimer's A beta(1--42) and A beta(25--35). *J Am Chem Soc* 2001, 123:5625-5631.
11. Jomova K, Vondrakova D, Lawson M, Valko M: Metals, oxidative stress and neurodegenerative disorders. *Mol Cell Biochem* 2010, 345:91-104.
12. Hutton M, Perez-Tur J, Hardy J: Genetics of Alzheimer's disease. *Essays Biochem* 1998, 33:117-131.
13. Younkin SG: The role of A beta 42 in Alzheimer's disease. *J Physiol Paris* 1998, 92:289-292.
14. Sisodia SS, Kim SH, Thinakaran G: Function and dysfunction of the presenilins. *Am J Hum Genet* 1999, 65:7-12.
15. Wang Y, Sheng G, Juranek S, Tuschl T, Patel DJ: Structure of the guide-strand-containing argonaute silencing complex. *Nature* 2008, 456:209-213.
16. Leuschner PJ, Ameres SL, Kueng S, Martinez J: Cleavage of the siRNA passenger strand during RISC assembly in human cells. *EMBO Rep* 2006, 7:314-320.
17. Schirle NT, MacRae IJ: The crystal structure of human Argonaute2. *Science* 2012, 336:1037-1040.
18. Lewis BP, Shih IH, Jones-Rhoades MW, Bartel DP, Burge CB: Prediction of mammalian microRNA targets. *Cell* 2003, 115:787-798.
19. Lai EC: Micro RNAs are complementary to 3' UTR sequence motifs that mediate negative post-transcriptional regulation. *Nat Genet* 2002, 30:363-364.
20. Selbach M, Schwanhausser B, Thierfelder N, Fang Z, Khanin R, Rajewsky N: Widespread changes in protein synthesis induced by microRNAs. *Nature* 2008, 455:58-63.
21. Baek D, Villen J, Shin C, Camargo FD, Gygi SP, Bartel DP: The impact of microRNAs on protein output. *Nature* 2008, 455:64-71.
22. Eulalio A, Huntzinger E, Izaurralde E: GW182 interaction with Argonaute is essential for miRNA-mediated translational repression and mRNA decay. *Nat Struct Mol Biol* 2008, 15:346-353.
23. Lee Y, Kim M, Han J, Yeom KH, Lee S, Baek SH, Kim VN: MicroRNA genes are transcribed by RNA polymerase II. *EMBO J* 2004, 23:4051-4060.
24. Han J, Lee Y, Yeom KH, Kim YK, Jin H, Kim VN: The Drosha-DGCR8 complex in primary microRNA processing. *Genes Dev* 2004, 18:3016-3027.
25. Yi R, Qin Y, Macara IG, Cullen BR: Exportin-5 mediates the nuclear export of pre-microRNAs and short hairpin RNAs. *Genes Dev* 2003, 17:3011-3016.

26. Bernstein E, Caudy AA, Hammond SM, Hannon GJ: Role for a bidentate ribonuclease in the initiation step of RNA interference. *Nature* 2001, 409:363-366.
27. Hutvagner G, McLachlan J, Pasquinelli AE, Balint E, Tuschl T, Zamore PD: A cellular function for the RNA-interference enzyme Dicer in the maturation of the let-7 small temporal RNA. *Science* 2001, 293:834-838.
28. Kim YK, Kim B, Kim VN: Re-evaluation of the roles of DROSHA, Export in 5, and DICER in microRNA biogenesis. *Proc Natl Acad Sci U S A* 2016, 113:E1881-1889.
29. Gao QQ, Putzbach W, Murmann AE, Chen S, Ambrosini G, Peter JM, Bartom E, Peter ME: 6mer seed toxicity in tumor suppressive miRNAs. *Nature Comm* 2018, 9:4504.
30. Hadji A, Ceppi P, Murmann AE, Brockway S, Pattanayak A, Bhinder B, Hau A, De Chant S, Parimi V, Kolesza P, et al: Death induced by CD95 or CD95 ligand elimination. *Cell Rep* 2014, 10:208-222.
31. Putzbach W, Gao QQ, Patel M, van Dongen S, Haluck-Kangas A, Sarshad AA, Bartom E, Kim KY, Scholtens DM, Hafner M, et al: Many si/shRNAs can kill cancer cells by targeting multiple survival genes through an off-target mechanism. *eLife* 2017, 6: e29702.
32. Patel M, Bartom ET, Paudel B, Kocherginsky M, O''Shea KL, Murmann AE, Peter ME: Identification of the toxic 6mer seed consensus in human cancer cells. *Sci Rep* 2022, 12:5130.
33. Stark A, Brennecke J, Bushati N, Russell RB, Cohen SM: Animal MicroRNAs confer robustness to gene expression and have a significant impact on 3'UTR evolution. *Cell* 2005, 123:1133-1146.
34. Murmann AE, Bartom ET, Schipma MJ, Vilker J, Chen S, Peter ME: 6mer seed toxicity in viral microRNAs. *iScience* 2019, 23: 100737.
35. Bartom ET, Kocherginsky M, Baudel B, Vaidyanathan A, Haluck-Kangas A, Patel M, O'Shea K, Murmann AE, Peter ME: SPOROS: A pipeline to analyze DISE/6mer seed toxicity. *PLOS Comp Biol* 2021, 18:e1010022.
36. Haluck-Kangas A, Patel M, Paudel B, Vaidyanathan A, Murmann AE, Peter MP: DISE/6mer Seed Toxicity - A powerful anti-cancer mechanism with implications for other diseases. *J Exp Clin Cancer Res* 2021, 40:389.
37. Landgraf P, Rusu M, Sheridan R, Sewer A, Iovino N, Aravin A, Pfeffer S, Rice A, Kamphorst AO, Landthaler M, et al: A mammalian microRNA expression atlas based on small RNA library sequencing. *Cell* 2007, 129:1401-1414.
38. Murmann AE, Gao QQ, Putzbach WT, Patel M, Bartom ET, Law CY, Bridgeman B, Chen S, McMahon KM, Thaxton CS, Peter ME: Small interfering RNAs based on huntingtin trinucleotide repeats are highly toxic to cancer cells. *EMBO Rep* 2018, 19:e45336.
39. Murmann AE, McMahon KM, Haluck-Kangas A, Ravindran N, Patel M, Law C, Brockway S, Wei JJ, Thaxton CS, Peter ME: Induction of DISE in ovarian cancer cells in vivo. *Oncotarget* 2017, 8:84643-84658.
40. Lu J, Getz G, Miska EA, varez-Saavedra E, Lamb J, Peck D, Sweet-Cordero A, Ebert BL, Mak RH, Ferrando AA, et al: MicroRNA expression profiles classify human cancers. *Nature* 2005, 435:834-838.
41. Putzbach W, Haluck-Kangas A, Gao QQ, Sarshad AA, Bartom ET, Stults A, Qadir AS, Hafner M, Peter ME: CD95/Fas ligand mRNA is toxic to cells. *eLife* 2018, 7:e38621.
42. Fa M, Orozco IJ, Francis YI, Saeed F, Gong Y, Arancio O: Preparation of oligomeric beta-amyloid 1-42 and induction of synaptic plasticity impairment on hippocampal slices. *J Vis Exp* 2010.
43. Stine WB, Jungbauer L, Yu C, LaDu MJ: Preparing synthetic Abeta in different aggregation states. *Methods Mol Biol* 2011, 670:13-32.
44. Krishtal J, Metsla K, Bragina O, Tõugu V, Palumaa P: Toxicity of Amyloid-β Peptides Varies Depending on Differentiation Route of SH-SY5Y Cells. *J Alzheimers Dis* 2019, 71:879-887.
45. Encinas M, Iglesias M, Liu Y, Wang H, Muhaisen A, Ceña V, Gallego C, Comella JX: Sequential treatment of SH-SY5Y cells with retinoic acid and brain-derived neurotrophic factor gives rise to fully differentiated, neurotrophic factor-dependent, human neuron-like cells. *J Neurochem* 2000, 75:991-1003.
46. Tagai N, Tanaka A, Sato A, Uchiumi F, Tanuma SI: Low Levels of Brain-Derived Neurotrophic Factor Trigger Self-aggregated Amyloid β-Induced Neuronal Cell Death in an Alzheimer's Cell Model. *Biol Pharm Bull* 2020, 43:1073-1080.
47. Oakley H, Cole SL, Logan S, Maus E, Shao P, Craft J, Guillozet-Bongaarts A, Ohno M, Disterhoft J, Van Eldik L, et al: Intraneuronal beta-amyloid aggregates, neurodegeneration, and neuron loss in transgenic mice with five familial Alzheimer's disease mutations: potential factors in amyloid plaque formation. *J Neurosci* 2006, 26:10129-10140.

48. Heckmann BL, Teubner BJW, Tummers B, Boada-Romero E, Harris L, Yang M, Guy CS, Zakharenko SS, Green DR: LC3-Associated Endocytosis Facilitates beta-Amyloid Clearance and Mitigates Neurodegeneration in Murine Alzheimer's Disease. *Cell* 2019, 178:536-551 e514.
49. McKhann GM, Knopman DS, Chertkow H, Hyman BT, Jack CR, Jr., Kawas CH, Klunk WE, Koroshetz WJ, Manly JJ, Mayeux R, et al: The diagnosis of dementia due to Alzheimer's disease: recommendations from the National Institute on Aging-Alzheimer's Association workgroups on diagnostic guidelines for Alzheimer's disease. *Alzheimers Dement* 2011, 7:263-269.
50. Hyman BT, Phelps CH, Beach TG, Bigio EH, Cairns NJ, Carrillo MC, Dickson DW, Duyckaerts C, Frosch MP, Masliah E, et al: National Institute on Aging-Alzheimer's Association guidelines for the neuropathologic assessment of Alzheimer's disease. *Alzheimers Dement* 2012, 8:1-13.
51. Rogalski EJ, Gefen T, Shi J, Samimi M, Bigio E, Weintraub S, Geula C, Mesulam MM: Youthful memory capacity in old brains: anatomic and genetic clues from the Northwestern SuperAging Project. *J Cogn Neurosci* 2013, 25:29-36.
52. Wadhwani AR, Affaneh A, Van Gulden S, Kessler JA: Neuronal apolipoprotein E4 increases cell death and phosphorylated tau release in alzheimer disease. *Ann Neurol* 2019, 85:726-739.
53. Zhang Y, Pak C, Han Y, Ahlenius H, Zhang Z, Chanda S, Marro S, Patzke C, Acuna C, Covy J, et al: Rapid single-step induction of functional neurons from human pluripotent stem cells. *Neuron* 2013, 78:785-798.
54. Mazzulli JR, Zunke F, Isacson O, Studer L, Krainc D: alpha-Synuclein-induced lysosomal dysfunction occurs through disruptions in protein trafficking in human midbrain synucleinopathy models. *Proc Natl Acad Sci U S A* 2016, 113:1931-1936.
55. Patel M, Wang Y, Bartom ET, Dhir R, Nephew KP, Matei D, Murmann AE, Lengyel E, Peter ME: The Ratio of Toxic-to-Nontoxic miRNAs Predicts Platinum Sensitivity in Ovarian Cancer. *Cancer Res* 2021, 81:3985-4000.
56. Hauptmann J, Schraivogel D, Bruckmann A, Manickavel S, Jakob L, Eichner N, Pfaff J, Urban M, Sprunck S, Hafner M, et al: Biochemical isolation of Argonaute protein complexes by Ago-APP. *Proc Natl Acad Sci U S A* 2015, 112:11841-11845.
57. Hafner M, Renwick N, Farazi TA, Mihailović A, Pena JTG, Tuschl T: Barcoded cDNA library preparation for small RNA profiling by next-generation sequencing. *Methods* 2012, 58:164-170.
58. Patel N, Hoang D, Miller N, Ansaloni S, Huang Q, Rogers JT, Lee JC, Saunders AJ: MicroRNAs can regulate human APP levels. *Mol Neurodegener* 2008, 3:10.
59. Feng MG, Liu CF, Chen L, Feng WB, Liu M, Hai H, Lu JM: MiR-21 attenuates apoptosis-triggered by amyloid-beta via modulating PDCD4/ PI3K/AKT/GSK-3beta pathway in SH-SY5Y cells. *Biomed Pharmacother* 2018, 101:1003-1007.
60. Higaki S, Muramatsu M, Matsuda A, Matsumoto K, Satoh JI, Michikawa M, Niida S: Defensive effect of microRNA-200b/c against amyloid-beta peptide-induced toxicity in Alzheimer's disease models. *PLoS One* 2018, 13:e0196929.
61. Lambert MP, Stevens G, Sabo S, Barber K, Wang G, Wade W, Krafft G, Snyder S, Holzman TF, Klein WL: Beta/A4-evoked degeneration of differentiated SH-SY5Y human neuroblastoma cells. *J Neurosci Res* 1994, 39:377-385.
62. Krishtal J, Bragina O, Metsla K, Palumaa P, Tougu V: In situ fibrillizing amyloid-beta 1-42 induces neurite degeneration and apoptosis of differentiated SH-SY5Y cells. *PLoS One* 2017, 12:e0186636.
63. Ferreira A, Busciglio J, Landa C, Caceres A: Ganglioside-enhanced neurite growth: evidence for a selective induction of high-molecular-weight MAP-2. *J Neurosci* 1990, 10:293-302.
64. Kaplan DR, Matsumoto K, Lucarelli E, Thiele CJ: Induction of TrkB by retinoic acid mediates biologic responsiveness to BDNF and differentiation of human neuroblastoma cells. Eukaryotic Signal Transduction Group. *Neuron* 1993, 11:321-331.
65. Patel M, Wang Y, Bartom ET, Dhir R, Nephew KP, Adli M, Matei D, Murmann AE, Lengyel E, Peter ME: The ratio of toxic-to-nontoxic microRNAs predicts platinum sensitivity in ovarian cancer. *Cancer Res* 2021, 81:3985-4000.
66. Tan GS, Chiu CH, Garchow BG, Metzler D, Diamond SL, Kiriakidou M: Small molecule inhibition of RISC loading. *ACS Chem Biol* 2012, 7:403-410.
67. Loo DT, Copani A, Pike CJ, Whittemore ER, Walencewicz AJ, Cotman CW: Apoptosis is induced by beta-amyloid in cultured central nervous system neurons. *Proc Natl Acad Sci U S A* 1993, 90:7951-7955.

68. Park H, Lee YB, Chang KA: miR-200c suppression increases tau hyperphosphorylation by targeting 14-3-3gamma in early stage of 5xFAD mouse model of Alzheimer's disease. *Int J Biol Sci* 2022, 18:2220-2234.
69. Martinez J, Malireddi RK, Lu Q, Cunha LD, Pelletier S, Gingras S, Orchard R, Guan JL, Tan H, Peng J, et al: Molecular characterization of LC3-associated phagocytosis reveals distinct roles for Rubicon, NOX2 and autophagy proteins. *Nat Cell Biol* 2015, 17:893-906.
70. Roberson ED, Scearce-Levie K, Palop JJ, Yan F, Cheng IH, Wu T, Gerstein H, Yu GQ, Mucke L: Reducing endogenous tau ameliorates amyloid beta-induced deficits in an Alzheimer's disease mouse model. *Science* 2007, 316:750-754.
71. Rapoport M, Dawson HN, Binder LI, Vitek MP, Ferreira A: Tau is essential to beta -amyloid-induced neurotoxicity. *Proc Natl Acad Sci U S A* 2002, 99:6364-6369.
72. Ferreira A, Bigio EH: Calpain-mediated tau cleavage: a mechanism leading to neurodegeneration shared by multiple tauopathies. *Mol Med* 2011, 17:676-685.
73. Lang AE, Riherd Methner DN, Ferreira A: Neuronal degeneration, synaptic defects, and behavioral abnormalities in tau(4)(5)(-)(2)(3)(0) transgenic mice. *Neuroscience* 2014, 275:322-339.
74. Sethi P, Lukiw WJ: Micro-RNA abundance and stability in human brain: Specific alterations in Alzheimer's disease temporal lobe neocortex. *Neuroscience Letters* 2009, 459:100-104.
75. Chen ML, Hong CG, Yue T, Li HM, Duan R, Hu WB, Cao J, Wang ZX, Chen CY, Hu XK, et al: Inhibition of miR-331-3p and miR-9-5p ameliorates Alzheimer's disease by enhancing autophagy. *Theranostics* 2021, 11:2395-2409.
76. Montine TJ, Phelps CH, Beach TG, Bigio EH, Cairns NJ, Dickson DW, Duyckaerts C, Frosch MP, Masliah E, Mirra SS, et al: National Institute on Aging-Alzheimer's Association guidelines for the neuropathologic assessment of Alzheimer's disease: a practical approach. *Acta Neuropathol* 2012, 123:1-11.
77. Greeve I, Hermans-Borgmeyer I, Brellinger C, Kasper D, Gomez-Isla T, Behl C, Levkau B, Nitsch RM: The human DIMINUTO/DWARF1 homolog seladin-1 confers resistance to Alzheimer's disease-associated neurodegeneration and oxidative stress. *J Neurosci* 2000, 20:7345-7352.
78. Bai X, Bian Z: MicroRNA-21 Is a Versatile Regulator and Potential Treatment Target in Central Nervous System Disorders. *Front Mol Neurosci* 2022, 15:842288.
79. Rossi RL, Rossetti G, Wenandy L, Curti S, Ripamonti A, Bonnal RJ, Birolo RS, Moro M, Crosti MC, Gruarin P, et al: Distinct microRNA signatures in human lymphocyte subsets and enforcement of the naive state in CD4+ T cells by the microRNA miR-125b. *Nat Immunol* 2011, 12:796-803.
80. Roy S: miRNA in Macrophage Development and Function. *Antioxid Redox Signal* 2016, 25:795-804.
81. Jovicic A, Roshan R, Moisoi N, Pradervand S, Moser R, Pillai B, Luthi-Carter R: Comprehensive expression analyses of neural cell-type-specific miRNAs identify new determinants of the specification and maintenance of neuronal phenotypes. *J Neurosci* 2013, 33:5127-5137.
82. Kosik KS: The neuronal microRNA system. *Nat Rev Neurosci* 2006, 7:911-920.
83. Schaefer A, O'Carroll D, Tan CL, Hillman D, Sugimori M, Llinas R, Greengard P: Cerebellar neurodegeneration in the absence of microRNAs. *J Exp Med* 2007, 204:1553-1558.
84. Davis TH, Cuellar TL, Koch SM, Barker AJ, Harfe BD, McManus MT, Ullian EM: Conditional loss of Dicer disrupts cellular and tissue morphogenesis in the cortex and hippocampus. *J Neurosci* 2008, 28:4322-4330.
85. Mori MA, Raghavan P, Thomou T, Boucher J, Robida-Stubbs S, Macotela Y, Russell SJ, Kirkland JL, Blackwell TK, Kahn CR: Role of microRNA processing in adipose tissue in stress defense and longevity. *Cell Metab* 2012, 16:336-347.
86. Mertens J, Reid D, Lau S, Kim Y, Gage FH: Aging in a Dish: iPSC-Derived and Directly Induced Neurons for Studying Brain Aging and Age-Related Neurodegenerative Diseases. *Annu Rev Genet* 2018, 52:271-293.
87. Min KW, Zealy RW, Davila S, Fomin M, Cummings JC, Makowsky D, McDowell CH, Thigpen H, Hafner M, Kwon SH, et al: Profiling of m6A RNA modifications identified an age-associated regulation of AGO2 mRNA stability. *Aging Cell* 2018, 17:e12753.
88. Musicco M, Adorni F, Di Santo S, Prinelli F, Pettenati C, Caltagirone C, Palmer K, Russo A: Inverse occurrence of cancer and Alzheimer disease: a population-based incidence study. *Neurology* 2013, 81:322-328.
89. Majd S, Power J, Majd Z: Alzheimer's Disease and Cancer: When Two Monsters Cannot Be Together. *Front Neurosci* 2019, 13:155.

90. Pan Y, Liu R, Terpstra E, Wang Y, Qiao F, Wang J, Tong Y, Pan B: Dysregulation and diagnostic potential of microRNA in Alzheimer's disease. *J Alzheimers Dis* 2016, 49:1-12.
91. Samadian M, Gholipour M, Hajiesmaeili M, Taheri M, Ghafouri-Fard S: The Eminent Role of microRNAs in the Pathogenesis of Alzheimer's Disease. *Front Aging Neurosci* 2021, 13:641080.
92. Flores O, Kennedy EM, Skalsky RL, Cullen BR: Differential RISC association of endogenous human microRNAs predicts their inhibitory potential. *Nucleic Acids Res* 2014, 42:4629-4639.
93. Jiang F, Ye X, Liu X, Fincher L, McKearin D, Liu Q: Dicer-1 and R3D1-L catalyze microRNA maturation in Drosophila. *Genes Dev* 2005, 19:1674-1679.
94. Bilen J, Liu N, Burnett BG, Pittman RN, Bonini NM: MicroRNA pathways modulate polyglutamine-induced neurodegeneration. *Mol Cell* 2006, 24:157-163.
95. Haramati S, Chapnik E, Sztainberg Y, Eilam R, Zwang R, Gershoni N, McGlinn E, Heiser PW, Wills AM, Wirguin I, et al: miRNA malfunction causes spinal motor neuron disease. *Proc Natl Acad Sci U S A* 2010, 107:13111-13116.
96. Schaefer A, Im HI, Veno MT, Fowler CD, Min A, Intrator A, Kjems J, Kenny PJ, O'Carroll D, Greengard P: Argonaute 2 in dopamine 2 receptor-expressing neurons regulates cocaine addiction. *J Exp Med* 2010, 207:1843-1851.
97. Bailey RR, Peddie BA: Enoxacin for the treatment of urinary tract infection. *N Z Med J* 1985, 98:286-288.
98. Shan G, Li Y, Zhang J, Li W, Szulwach KE, Duan R, Faghihi MA, Khalil AM, Lu L, Paroo Z, et al: A small molecule enhances RNA interference and promotes microRNA processing. *Nat Biotechnol* 2008, 26:933-940.
99. Melo S, Villanueva A, Moutinho C, Davalos V, Spizzo R, Ivan C, Rossi S, Setien F, Casanovas O, Simo-Riudalbas L, et al: Small molecule enoxacin is a cancer-specific growth inhibitor that acts by enhancing TAR RNA-binding protein 2-mediated microRNA processing. *Proc Natl Acad Sci U S A* 2011, 108:4394-4399.
100. Emde A, Eitan C, Liou LL, Libby RT, Rivkin N, Magen I, Reichenstein I, Oppenheim H, Eilam R, Silvestroni A, et al: Dysregulated miRNA biogenesis downstream of cellular stress and ALS-causing mutations: a new mechanism for ALS. *EMBO J* 2015, 34:2633-2651.
101. Chmielarz P, Konovalova J, Najam SS, Alter H, Piepponen TP, Erfle H, Sonntag KC, Schutz G, Vinnikov IA, Domanskyi A: Dicer and microRNAs protect adult dopamine neurons. *Cell Death Dis* 2017, 8:e2813.
102. Putzbach W, Gao QQ, Patel M, Haluck-Kangas A, Murmann AE, Peter ME: DISE - A Seed Dependent RNAi Off-Target Effect that Kills Cancer Cells. *Trends in Cancer* 2018, 4:10-19.
103. Ungvari Z, Tucsek Z, Sosnowska D, Toth P, Gautam T, Podlutsky A, Csiszar A, Losonczy G, Valcarcel-Ares MN, Sonntag WE, Csiszar A: Aging-induced dysregulation of dicer1-dependent microRNA expression impairs angiogenic capacity of rat cerebromicrovascular endothelial cells. *J Gerontol A, Biol Sci Med Sci* 2013, 68:877-891.
104. Inukai S, de Lencastre A, Turner M, Slack F: Novel microRNAs differentially expressed during aging in the mouse brain. *PLoS One* 2012, 7:e40028.
105. Wiesen JL, Tomasi TB: Dicer is regulated by cellular stresses and interferons. *Mol Immunol* 2009, 46:1222-1228.
106. Machitani M, Sakurai F, Wakabayashi K, Takayama K, Tachibana M, Mizuguchi H: Type I Interferons Impede Short Hairpin RNA-Mediated RNAi via Inhibition of Dicer-Mediated Processing to Small Interfering RNA. *Mol Ther Nucleic Acids* 2017, 6:173-182.
107. Hengst U, Cox LJ, Macosko EZ, Jaffrey SR: Functional and selective RNA interference in developing axons and growth cones. *J Neurosci* 2006, 26:5727-5732.
108. Khachaturian AS, Hayden KM, Mielke MM, Tang Y, Lutz MW, Gustafson DR, Kukull WA, Mohs R, Khachaturian ZS: Future prospects and challenges for Alzheimer's disease drug development in the era of the NIA-AA Research Framework. *Alzheimers Dement* 2018, 14:532-534.

Figure 1

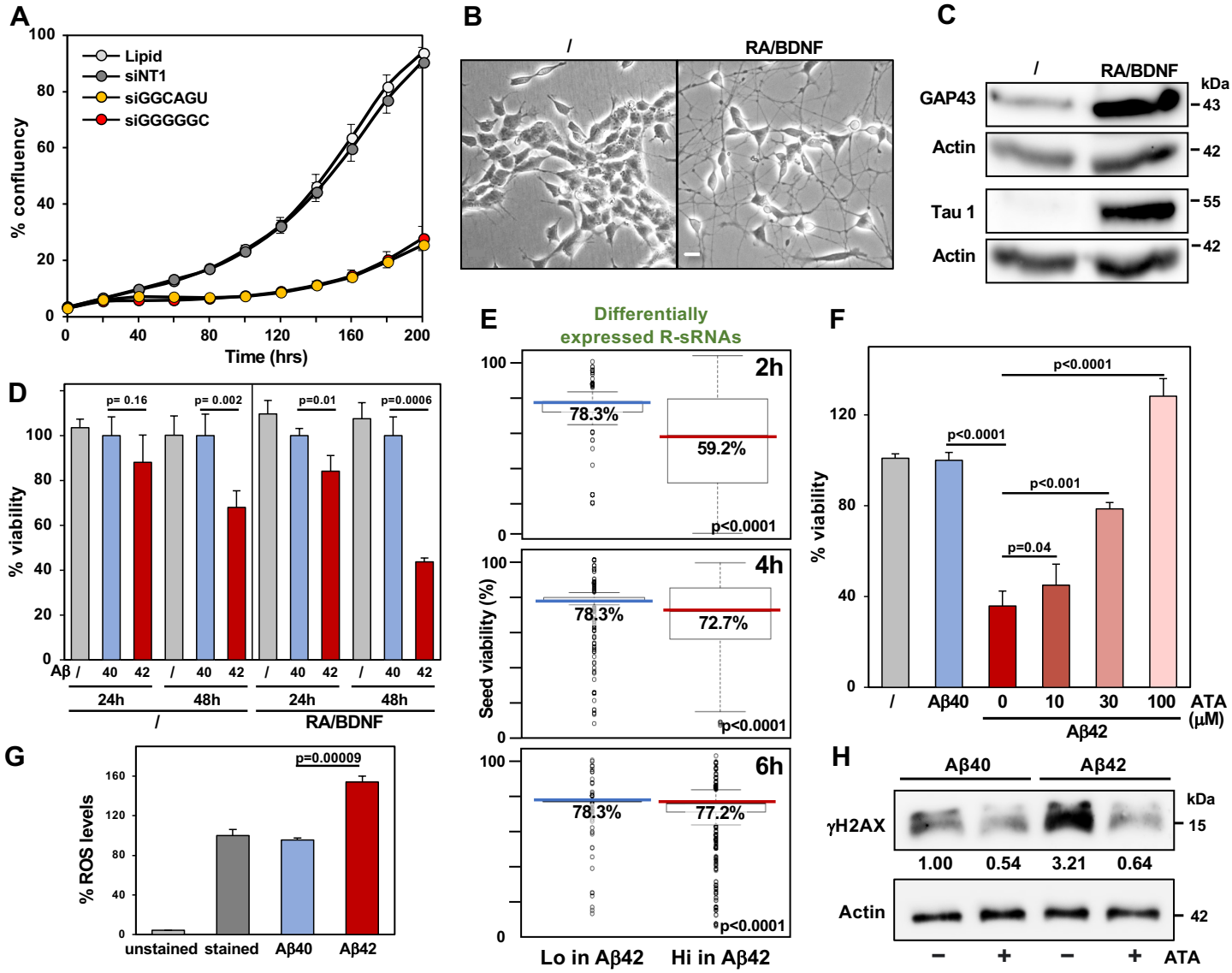

Fig. 2

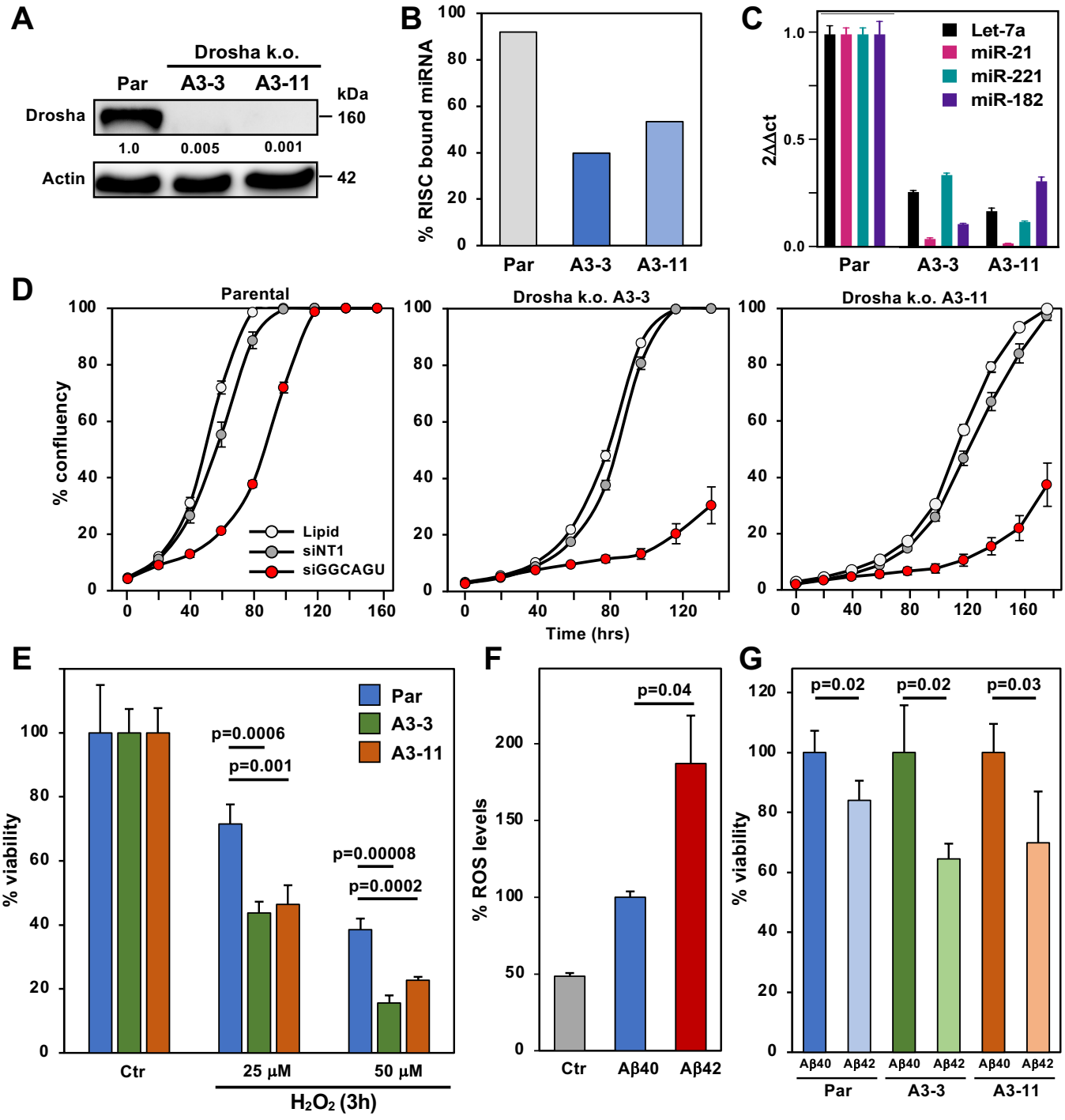

Figure 3

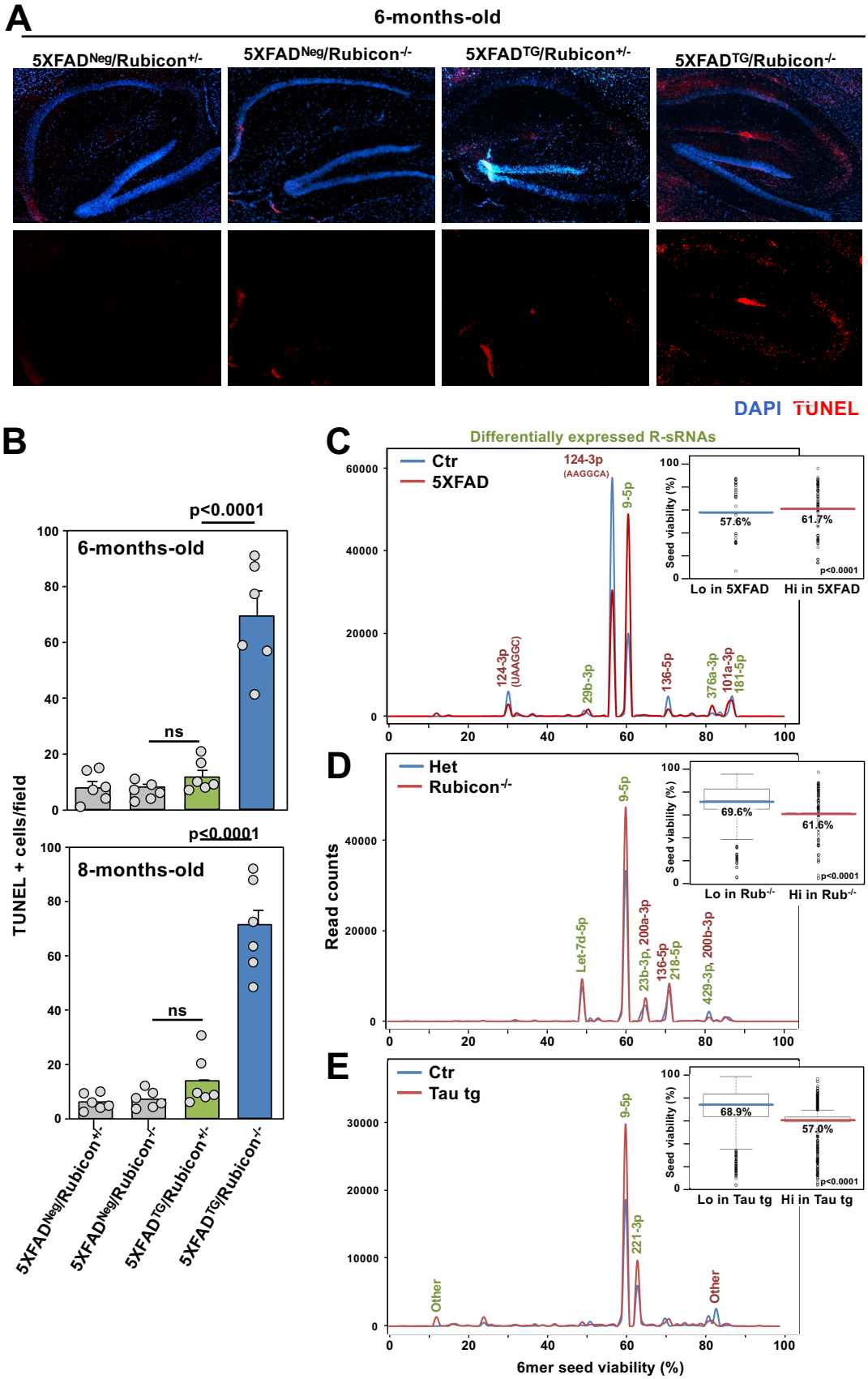

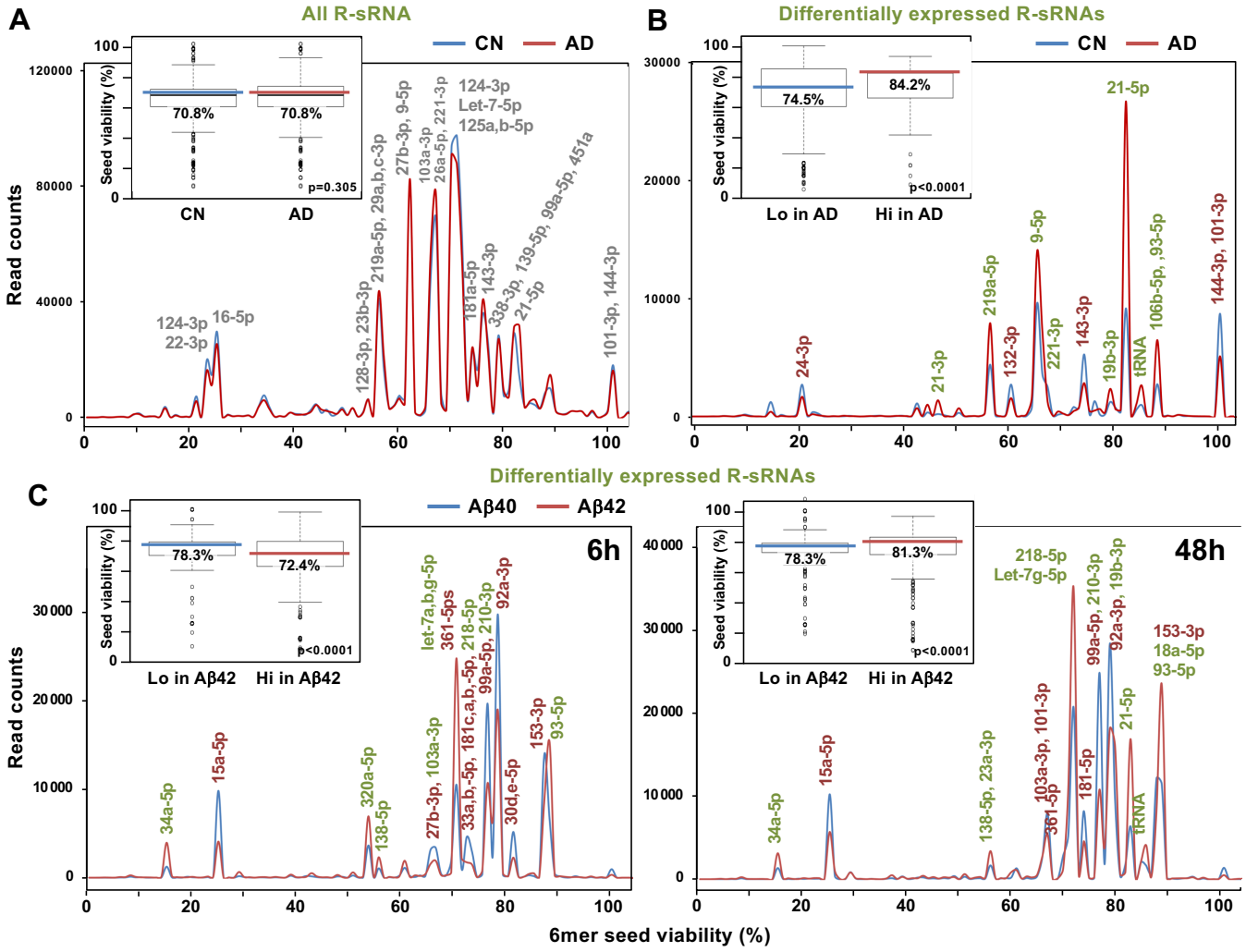
A
All R-sRNA
CN
AD
Read counts
Seed viability (%)
70.8%
70.8%
p=0.305
CN
AD
124-3p
16-5p
22-3p
128-3p, 23b-3p
219a-5p, 29a,b,c-3p
27b-3p, 9-5p
103a-3p
26a-5p, 221-3p
124-3p
Let-7-5p
125a,b-5p
181a-5p
143-3p
338-3p, 139-5p, 99a-5p, 451a
21-5p
101-3p, 144-3p
B
Differentially expressed R-sRNAs
CN
AD
74.5%
84.2%
p<0.0001
Lo in AD
Hi in AD
24-3p
21-3p
219a-5p
132-3p
9-5p
221-3p
143-3p
19b-3p
tRNA
21-5p
106b-5p, 93-5p
144-3p, 101-3p
C
Differentially expressed R-sRNAs
Aβ40
Aβ42
6h
78.3%
72.4%
p<0.0001
Lo in Aβ42
Hi in Aβ42
34a-5p
15a-5p
320a-5p
138-5p
27b-3p, 103a-3p
let-7a,b,g-5p
361-5ps
218-5p
33a,b,-5p, 181c,a,b,-5p
99a-5p, 210-3p
92a-3p
30d,e-5p
153-3p
93-5p
48h
78.3%
81.3%
p<0.0001
Lo in Aβ42
Hi in Aβ42
218-5p
Let-7g-5p
99a-5p, 210-3p
92a-3p, 19b-3p
153-3p
18a-5p
93-5p
34a-5p
15a-5p
138-5p, 23a-3p
103a-3p, 101-3p
361-5p
181-5p
21-5p
tRNA
6mer seed viability (%)

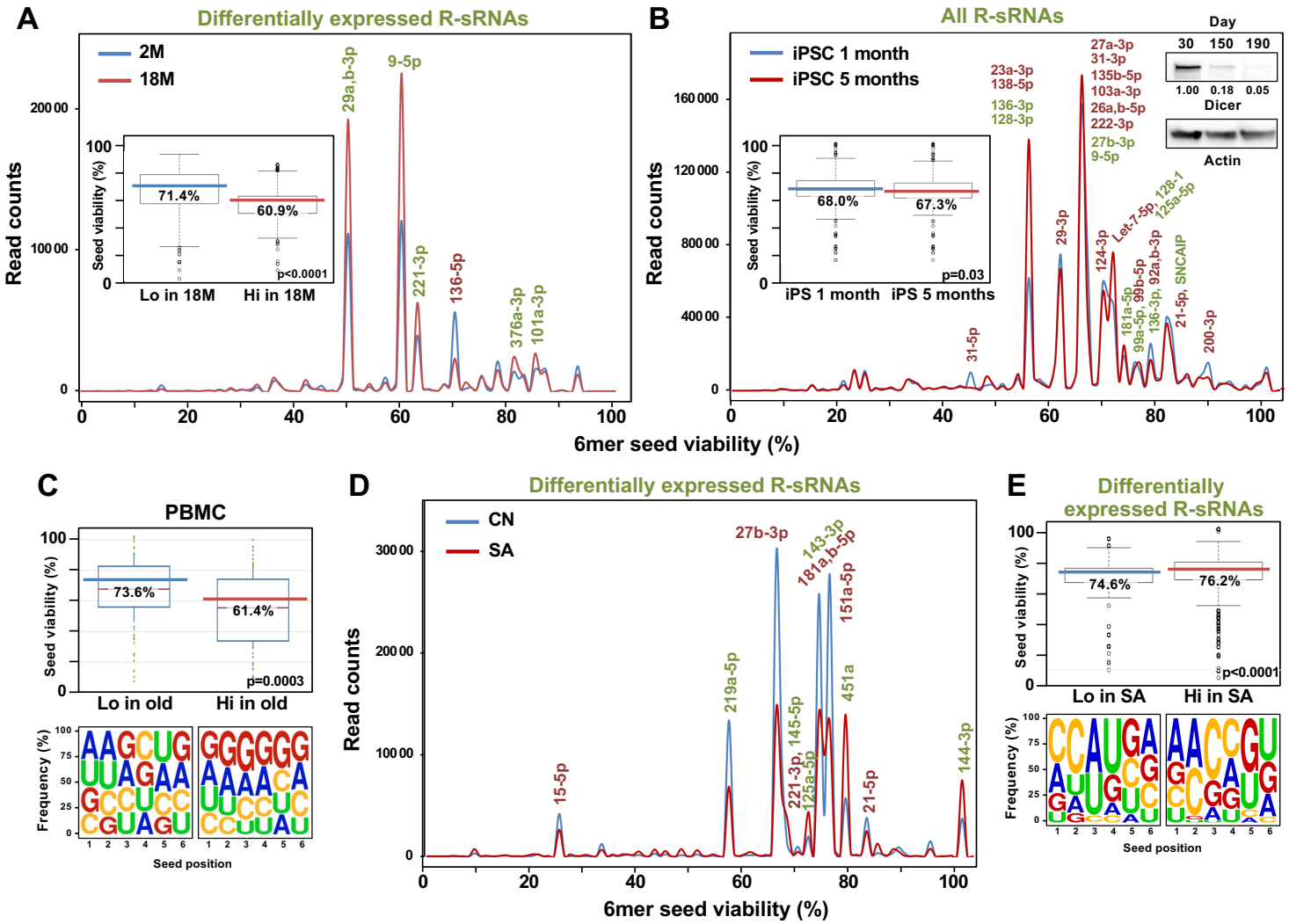
A
Differentially expressed R-sRNAs
2M
18M
29a,b-3p
9-5p
221-3p
136-5p
376a-3p
101a-3p
Seed viability (%)
71.4%
60.9%
p<0.0001
Lo in 18M
Hi in 18M
Read counts
6mer seed viability (%)
B
All R-sRNAs
iPSC 1 month
iPSC 5 months
Day
30 150 190
1.00 0.18 0.05
Dicer
Actin
27a-3p
31-3p
135b-5p
103a-3p
26a,b-5p
222-3p
27b-3p
9-5p
23a-3p
138-5p
136-3p
128-3p
29-3p
124-3p
Let-7-5p, 128-1
125a-5p
181a-5p
99a-5p, 99b-5p
136-3p, 92a,b-3p
21-5p, SNCAIP
200-3p
31-5p
68.0%
67.3%
p=0.03
iPS 1 month
iPS 5 months
C
PBMC
73.6%
61.4%
p=0.0003
Lo in old
Hi in old
Frequency (%)
Seed position
D
Differentially expressed R-sRNAs
CN
SA
27b-3p
143-3p
181a,b-5p
151a-5p
219a-5p
145-5p
451a
221-3p, 125a-5p
21-5p
144-3p
15-5p
E
Differentially expressed R-sRNAs
74.6%
76.2%
p<0.0001
Lo in SA
Hi in SA

Figure 6

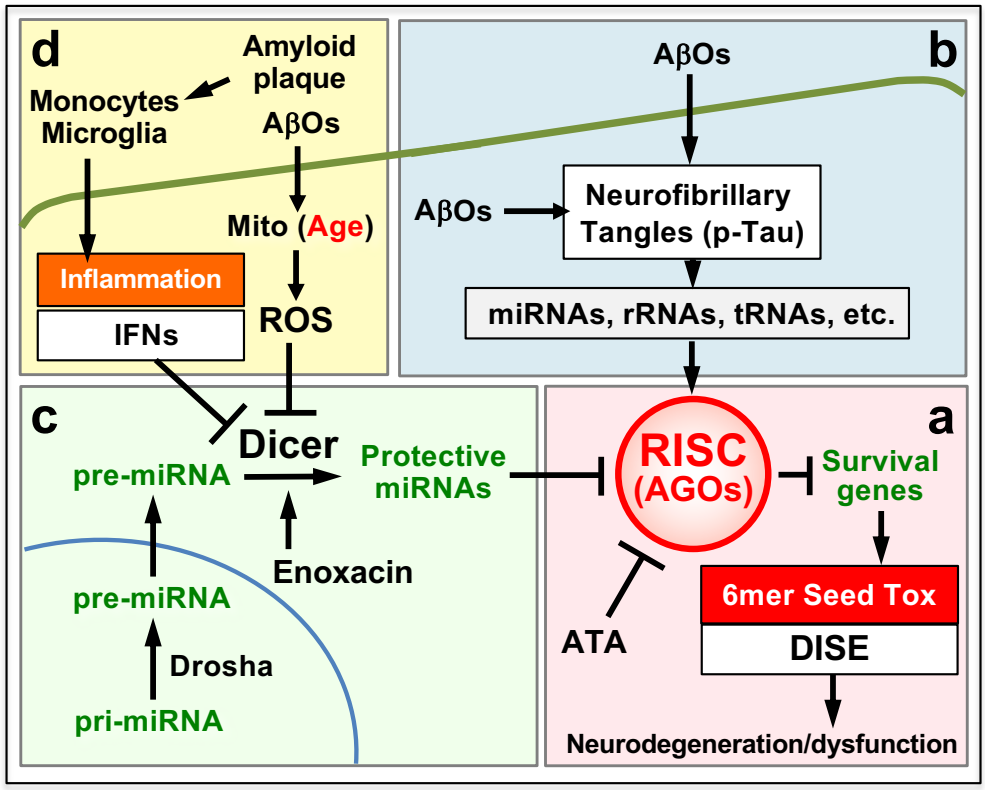

Figure S1

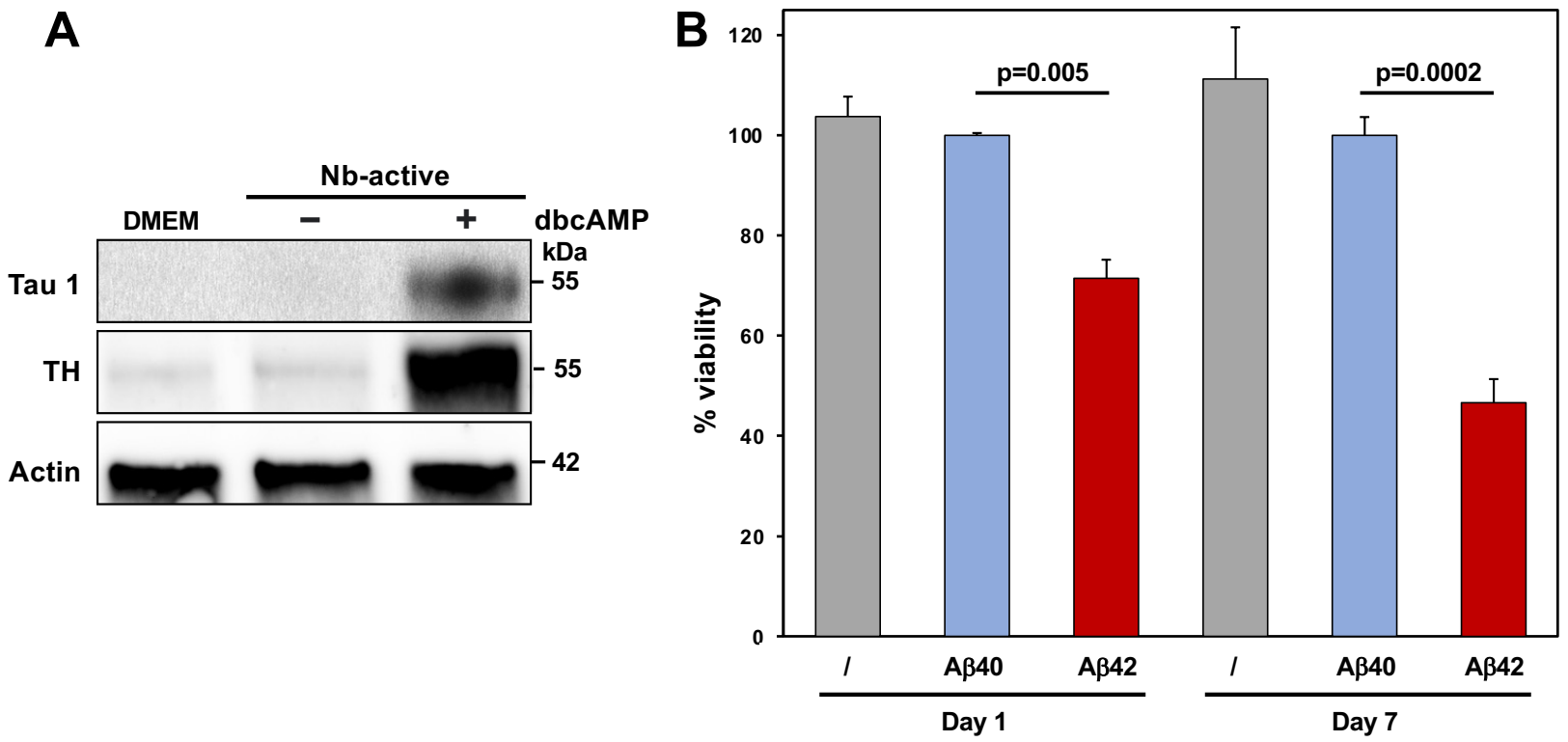
A
Nb-active
DMEM
–
+
dbcAMP
kDa
Tau 1
55
TH
55
Actin
42
B
% viability
120
100
80
60
40
20
0
p=0.005
p=0.0002
/
Aβ40
Aβ42
/
Aβ40
Aβ42
Day 1
Day 7

Figure S2

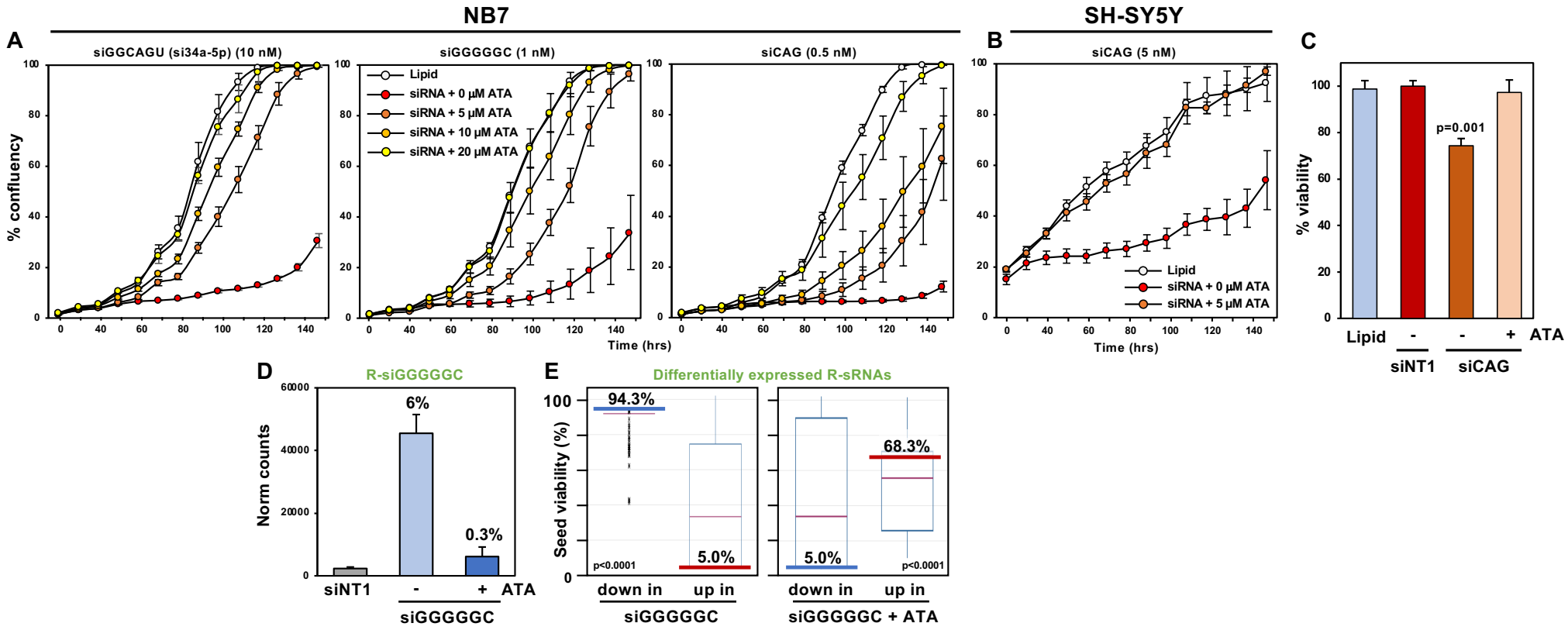
NB7
A
siGGCAGU (si34a-5p) (10 nM)
siGGGGGC (1 nM)
siCAG (0.5 nM)
% confluency
Time (hrs)
Lipid
siRNA + 0 µM ATA
siRNA + 5 µM ATA
siRNA + 10 µM ATA
siRNA + 20 µM ATA
SH-SY5Y
B
siCAG (5 nM)
C
% viability
p=0.001
Lipid
siNT1
siCAG
ATA
D
R-siGGGGGC
Norm counts
6%
0.3%
siNT1
siGGGGGC
E
Differentially expressed R-sRNAs
Seed viability (%)
94.3%
5.0%
p<0.0001
68.3%
down in
up in
siGGGGGC + ATA

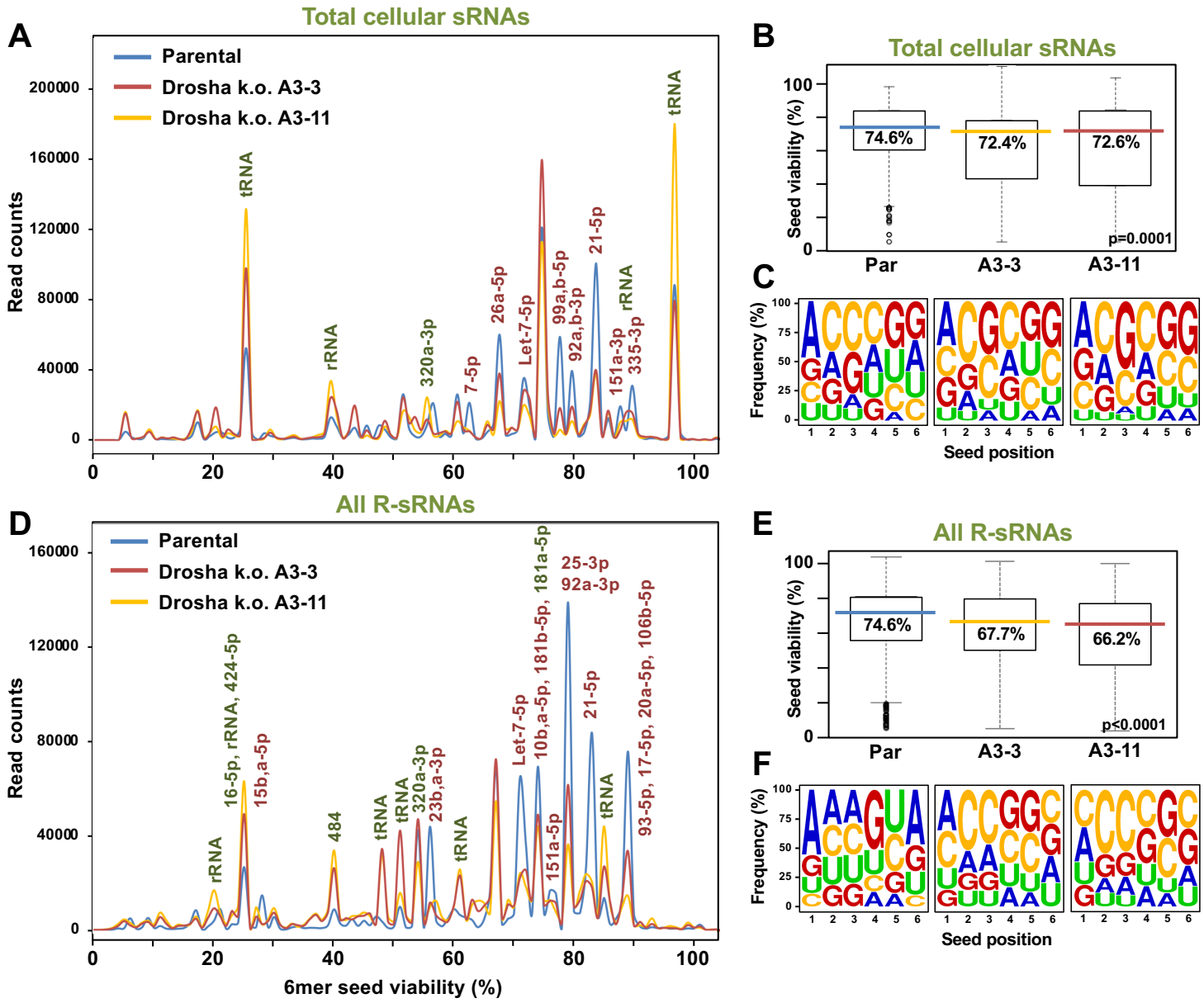
A
Total cellular sRNAs
Parental
Drosha k.o. A3-3
Drosha k.o. A3-11
Read counts
tRNA
rRNA
320a-3p
7-5p
26a-5p
Let-7-5p
99a,b-5p
92a,b-3p
21-5p
151a-3p
335-3p
rRNA
tRNA
B
Total cellular sRNAs
Seed viability (%)
74.6%
72.4%
72.6%
p=0.0001
Par
A3-3
A3-11
C
Frequency (%)
Seed position
D
All R-sRNAs
Parental
Drosha k.o. A3-3
Drosha k.o. A3-11
Read counts
rRNA
16-5p, rRNA, 424-5p
15b,a-5p
484
tRNA
tRNA
320a-3p
23b,a-3p
tRNA
Let-7-5p
10b,a-5p, 181b-5p, 181a-5p
151a-5p
25-3p
92a-3p
21-5p
tRNA
93-5p, 17-5p, 20a-5p, 106b-5p
6mer seed viability (%)
E
All R-sRNAs
Seed viability (%)
74.6%
67.7%
66.2%
p≤0.0001
Par
A3-3
A3-11
F
Frequency (%)
Seed position

Figure S4

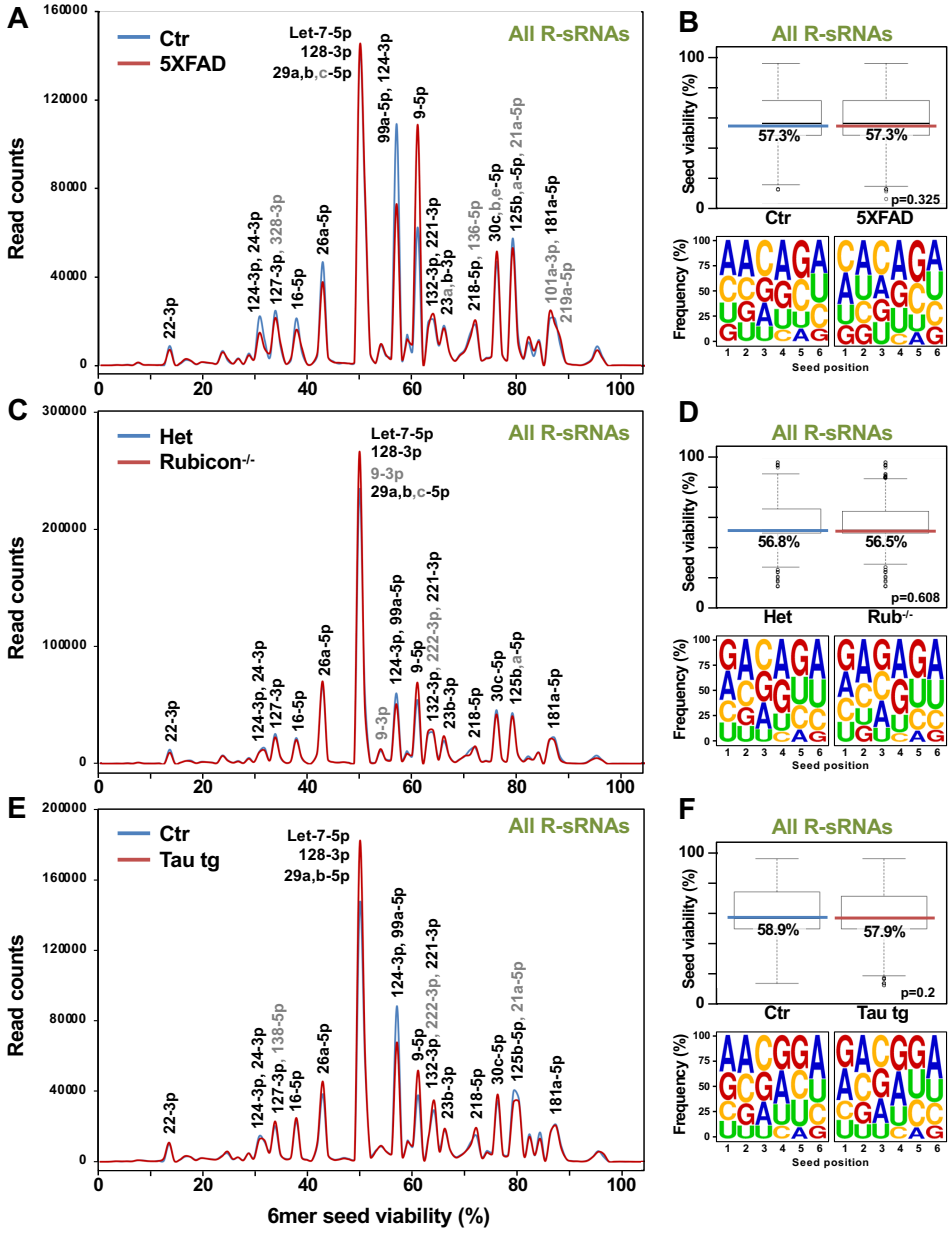

Figure S5

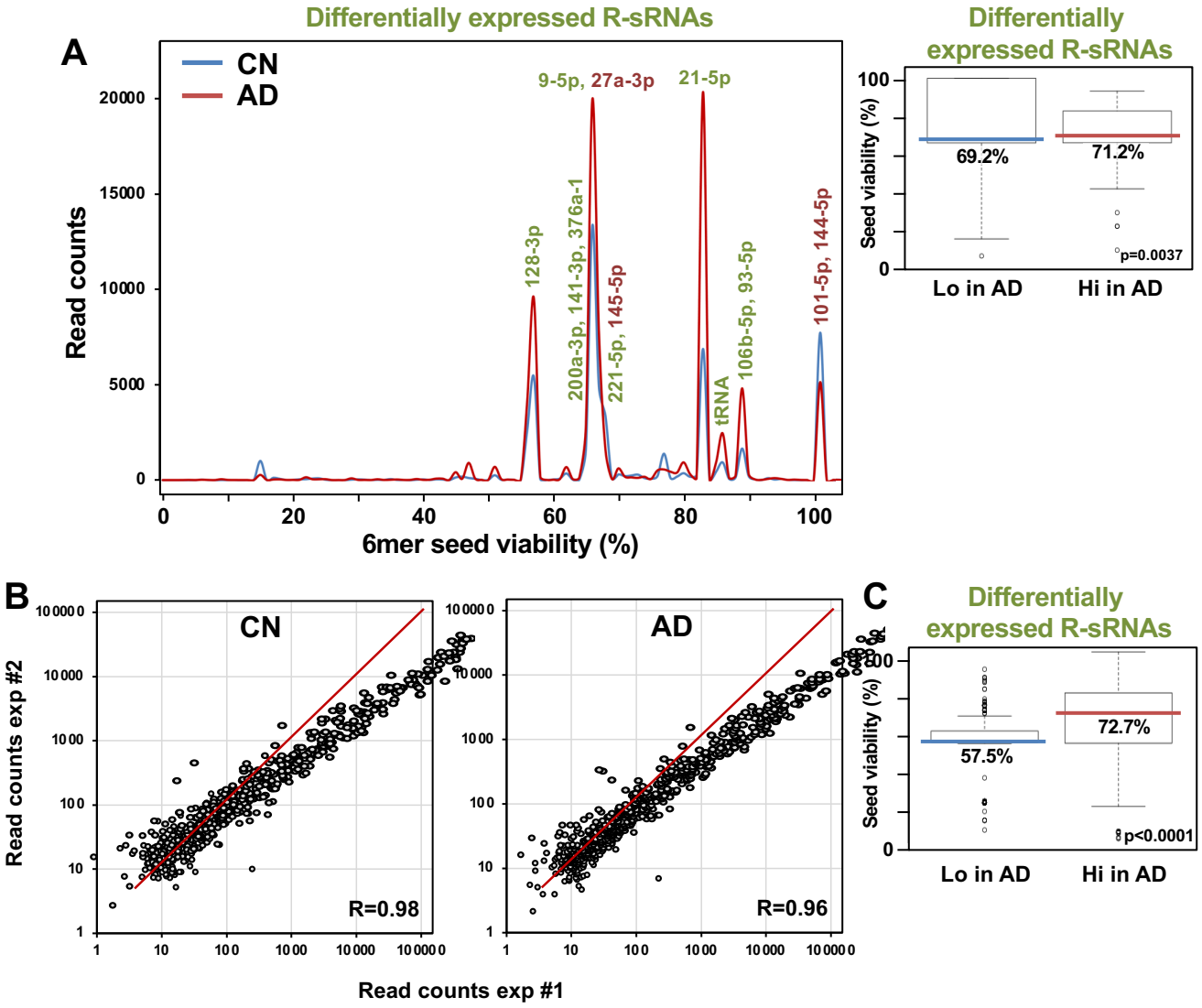

Figure S6

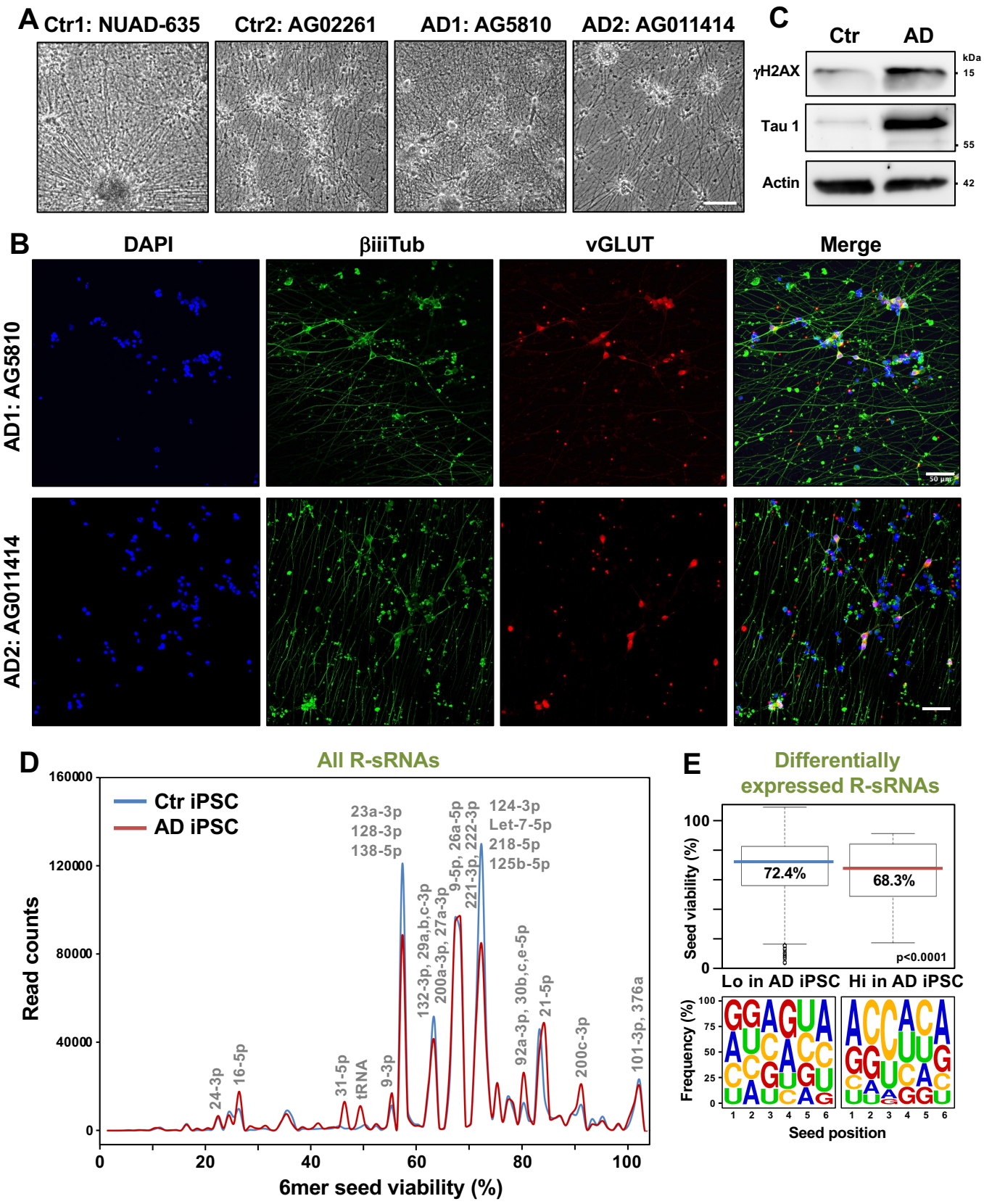

Figure S7

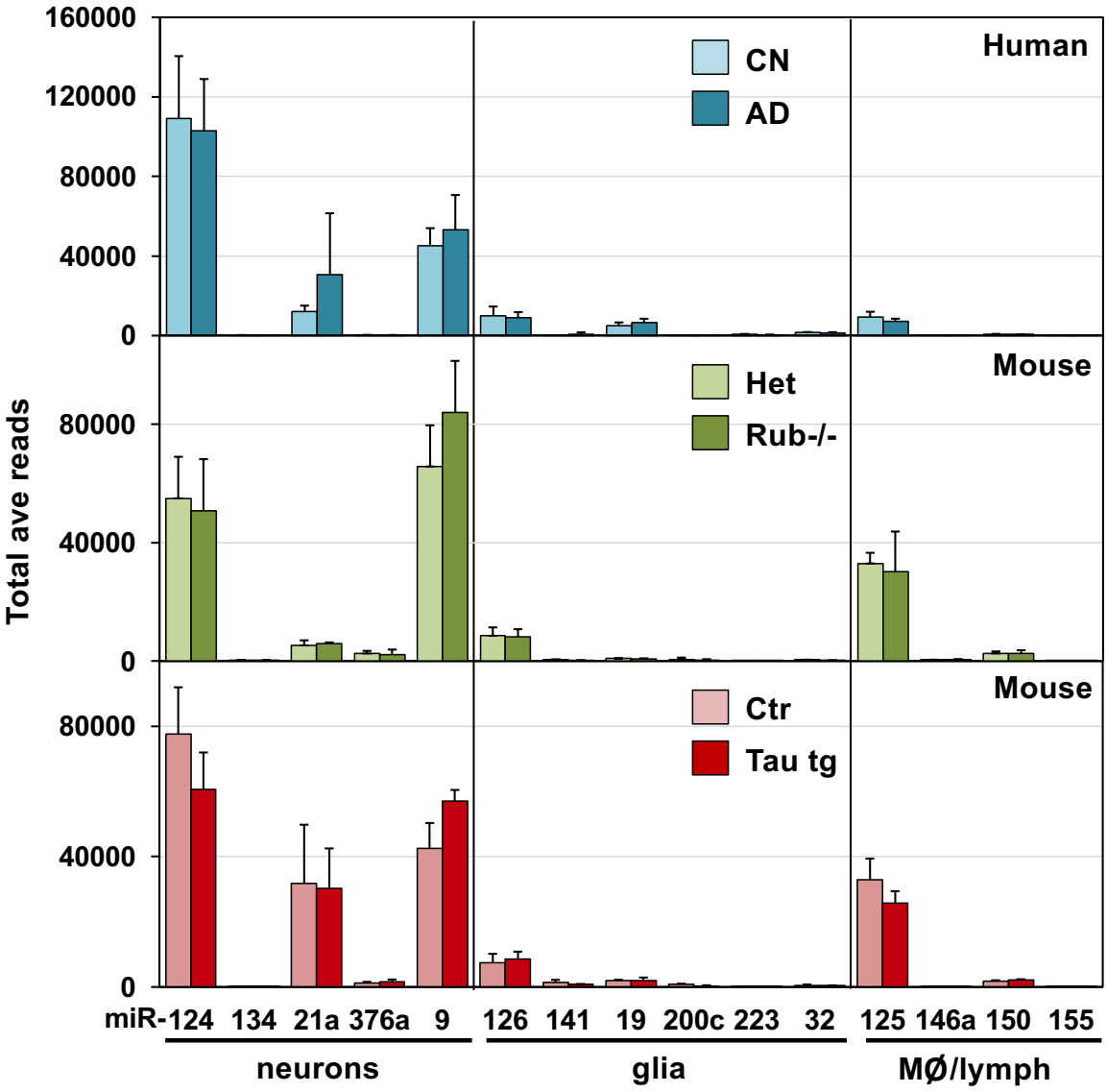

Figure S8

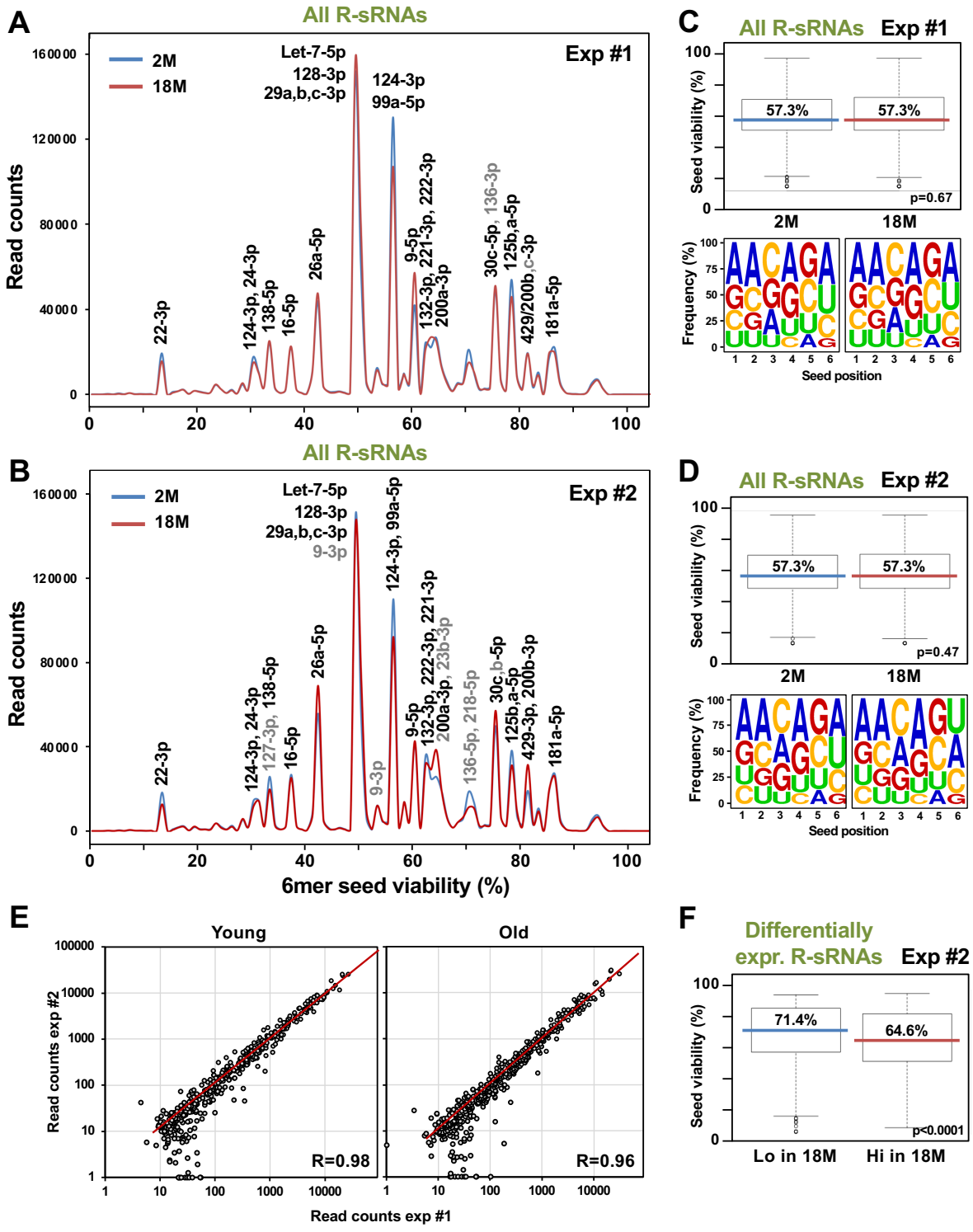

Figure S9

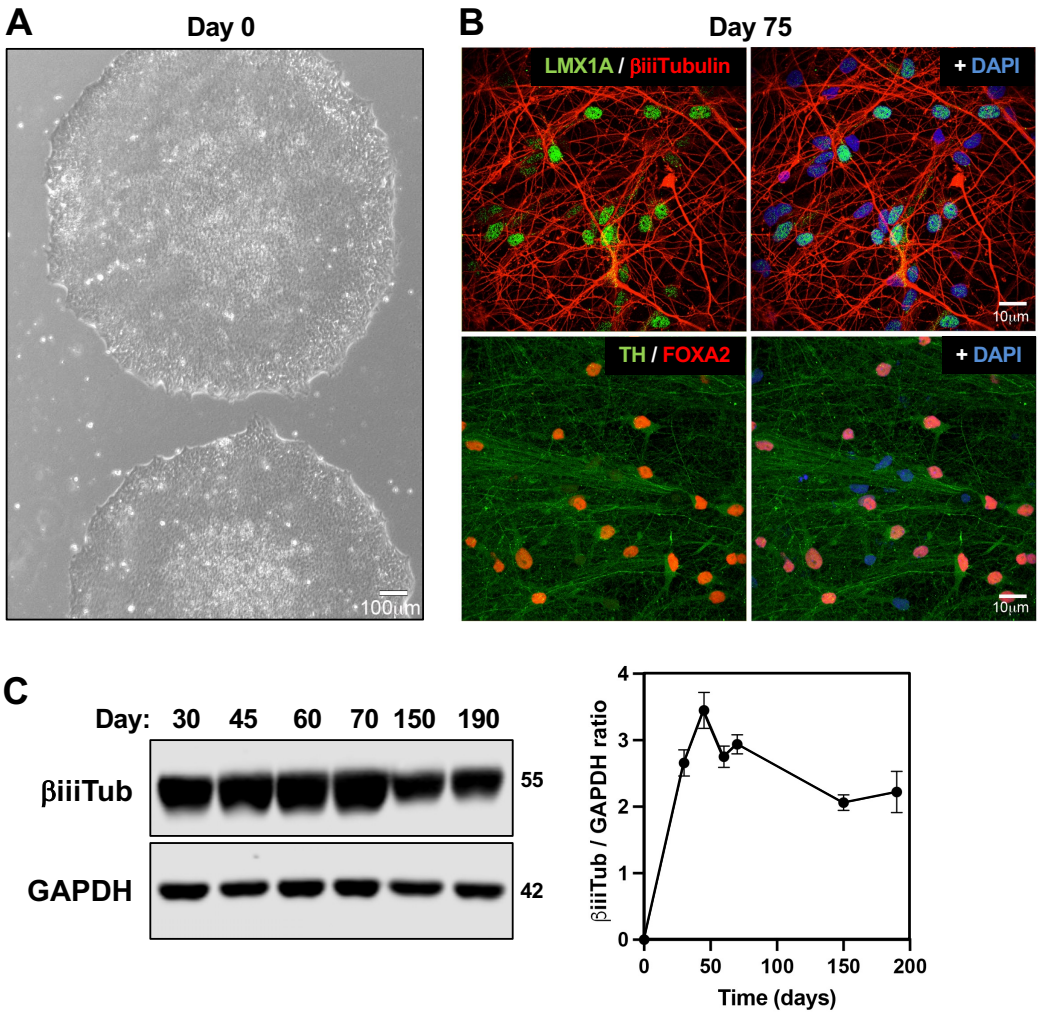

Figure S10